Journal of South American Earth Sciences 73 (2017) 78–99

Contents lists available at ScienceDirect

Journal of South American Earth Sciences

journal homepage: www.elsevier.com/locate/jsames

Vestiges of a continental margin ophiolite type in the Novo Oriente region, Borborema Province, NE Brazil

João Paulo Araújo Pitombeira [a, *], Wagner da Silva Amaral [a], Evilarde Carvalho Uchôa Filho [b], Reinhardt Adolfo Fuck [c], Elton Luiz Dantas [c], Clóvis Vaz Parente [d], Felipe Grandjean da Costa [b], César Ulisses Vieira Veríssimo [d]

[a] Instituto de Geociências, Universidade Estadual de Campinas, 13081-970, Campinas, SP, Brazil
[b] Geological Survey of Brazil, Brazil
[c] Instituto de Geociências, Universidade de Brasília, 70910-900, Brasília, DF, Brazil
[d] Departamento de Geologia, Universidade Federal do Ceará, Fortaleza, CE, Brazil

ARTICLE INFO

Article history:
Received 17 July 2016
Received in revised form
16 November 2016
Accepted 27 November 2016
Available online 30 November 2016

Keywords:
Novo oriente
Metaultramafic rocks
Metamafic rocks
Geochemistry
CM Ophiolite type

ABSTRACT

The Novo Oriente Group is a restricted well-preserved metasedimentary sequence, composed of two tectonic-stratigraphic sequences in the southwestern portion of the Ceará Central Domain, NE Brazil. The Bonsucesso Formation comprises mainly quartzite and metamafic rocks and the Caraúbas Formation is dominantly metapelitic, with chemical sedimentary contribution, metamafic and metaultramafic rocks. New integrated field, geochemical data and Sm-Nd isotopes of the metaultramafic and metamafic rocks of the two formations have been investigated in order to determine their tectonic setting. The metaultramafic rocks are dominantly composed of deformed and undeformed serpentinites, chloritites, actinolitites, talc-chlorite schists, serpentine-talc schists, talc-rich siliceous rocks and subordinated listwänites. Geochemical data indicate that the serpentinites correspond to rocks resulting from the alteration of dunites depleted in HREE, similar to the pattern presented by subduction-zone serpentinites generated from exhumed sub-continental peridotites and hydrated during ocean-continent transition (OCT) rifting. The metamafic rocks, represented by metagabbros, hornblende metagabbros and metabasalts, consist of basic rocks of basaltic and tholeiitic affinity with signatures between E- and N-MORB and variable contamination by crustal components similar to the rocks formed from the interaction between mantle plumes and heavily thinned continental crust. Isotopic analysis indicates crustal assimilation with negative εNd and Paleoproterozoic T_{DM} ages. The data suggest that metaultramafic and metamafic rocks correspond, respectively, to continental sub-lithospheric mantle exhumed in an area of ocean-continent transition (OCT), and mafic magmatism associated with the development of a magma-poor passive margin generated by the break-up of the Rodinia Supercontinent, which was later dismembered by the Brasiliano/Pan-African Orogeny collisional phase and preserved as a Continental Margin Ophiolite type.

1. Introduction

Ophiolites are suites formed of ultramafic, mafic and felsic rocks, interpreted as remnants of oceanic crust and upper mantle that are temporally and spatially associated in specific tectonic environments, and constitute an important piece of evidence to the understanding of tectonic and magmatic processes of the oceanic lithosphere through time (Dilek and Furnes, 2014). Between the Archean and the Mesoproterozoic record of ophiolitic sequences is scarce due to events of intense crustal deformation and reworking along geological time, often causing disruption of the original sequences (Dilek and Furnes, 2011; Furnes et al., 2013). The best-preserved Precambrian ophiolitic sequences correspond to Neoproterozoic ophiolites, which were recorded mainly in Africa, South America, Arabia, Europe, Central Asia and northwestern India (e.g., Moores, 2002; Dilek and Robinson, 2003).

Several studies focus on Neoproterozoic ophiolites recorded in orogenic belts of Gondwana, as for example in the Egypt Desert, in

* Corresponding author.
E-mail address: joao_pauloap@hotmail.com (J.P.A. Pitombeira).

http://dx.doi.org/10.1016/j.jsames.2016.11.007
0895-9811/

the Um Salim-Um Salatit (Salem et al., 2012), El Ideid-El Sodmein (Farahat, 2008), and Bir Al-Edeid (Azer and Khalil, 2005) regions, in Morocco, in the Bou Azzer Anti Atlas (Bodinier et al., 1984; Ahmed et al., 2005; Bousquet et al., 2008), Arabian–Nubian ophiolites (Stern et al., 2004; Johnson et al., 2004) and the Timétrine massif in northeastern Mali (Caby, 2014). Record of ophiolitic sequences in Brazil are similar to the occurrences in the Egypt Desert and are represented by plutonic metaultramafic rocks tectonically intercalated with metavolcano-sedimentary or metasedimentary sequences of varying metamorphic grade, from greenschist to amphibolite facies. The main records in Brazil are of Neoproterozoic age, occurring in the Araçuaí, Brasília, Araguaia and Ribeira belts (e.g., Pedrosa-Soares et al., 1998; Tassinari et al., 2001; Suíta et al., 2004; Queiroga et al., 2007, 2012; Paixão et al., 2008; Paixão, 2009).

Ophiolitic sequences are classified as subduction-related ophiolites and subduction-unrelated ophiolites (Dilek and Furnes, 2011). The subduction-related ophiolites include suprasubduction zone type and volcanic arc type. The subduction-unrelated ophiolites include continental-margin-, mid ocean-ridge, and plume type ophiolites. Continental Margin Ophiolites are fragments of magma-poor passive margins, ocean-continent transitions (OCT's). These ofiolites are characterized by sub-continental mantle fragments, generally of harzburgitic or dunitic composition, associated with intrusive and extrusive mafic rocks and magma-poor passive margin sediments (Boillot and Froitzheim, 2001; Manatschal and Müntener, 2009; Reston and Manatschal, 2011).

Passive margins are directly related to the opening of an ocean, where the width and structure depend on several factors. During the formation of a passive margin abundant magmatism can or cannot occur. When there is the generation of a small volume of volcanic rocks, the passive margin is characterized as magma-poor (magma-poor passive margin, Reston, 1993; Manatschal, 2004; Franke, 2013). In this case, mantle rocks can exposed in the oceanic floor and due to the process of oceanic-floor metamorphism, the mantle rocks, generally of harzburgitic composition, undergo strong serpentinization.

The formation of magma-poor passive margins takes place in extensional regime and consistently presents extreme crustal thinning accompanied by normal faulting, serpentinization of the upper mantle located bellow the crust (2–8 km in depth) and exhumation of a large continental mantle zone in the continent-oceanic crust transition, accompanied by the development of a detachment surface and faults with large displacements, and intrusive and extrusive mafic magmatism (Reston, 2009; Whitmarsh and Manatschal, 2012).

The mafic magmatism associated with this faulting and formation of embryonic oceanic crust is represented by gabbroic and basaltic crustal rocks with MORB geochemical signature that range in composition and spatial distribution along the ocean-continent transition (OCT, Whitmarsh et al., 2001). Mafic rocks with T-MORB signatures occur closer to the continental margin while N-MORB signatures are found predominantly toward the ocean and in greater volume (Desmurs et al., 2002).

In this paper we report field observations, geochemical and whole rock Sm-Nd data on the metaultramafic and metamafic rocks from the Novo Oriente Group, southwestern Ceará Central Domain (Northeast Brazil). These data provide new insights into the genetic settings of the metaultramafic and metamafic rocks in this region during the tectonic evolution of Western Gondwana.

2. Geological setting

The study area is located in the Ceará Central Domain – CCD, in the northern portion of the Borborema Province (Almeida et al., 1981; Caby, 1989; Brito Neves and Cordani, 1991; Trompette, 1994; El Hadji et al., 1997; Fetter et al., 2000; Tack et al., 2001; Van Schmus et al., 2011), northeastern part of the South-American Platform (Fig. 1).

The Borborema Province is a complex region of tectonic and stratigraphic domains, marked by thermal-tectonic events of various ages, the most important of which is the Neoproterozoic Brasiliano/Pan-African Orogeny. The present Borborema Province configuration resulted from the Brasiliano/Pan-African Orogeny as a consequence of the convergence of the Amazonian-São Luís-West Africa and São Francisco-Congo cratons and other minor blocks, during the formation of West Gondwana.

The Ceará Central Domain is constituted of: 1) Archean remains (3.2–2.7 Ga) of TTG-affinity (tonalite-trondhjemite-granodiorite) that belong to the Cruzeta Complex; 2) Migmatized, intermediate to silicic orthogneisses, including supracrustal rocks, and Paleoproterozoic rocks of juvenile character (2.1–2.2 Ga, Fetter et al., 2000; Martins et al., 2009); 3) Paleo- to Neoproterozoic, high-grade supracrustal rocks, represented in part by units of the Ceará Complex and Novo Oriente Group (Arthaud, 2008; Ganade de Araújo et al., 2010); 4) Neoproterozoic granitoids that constitute the Santa Quitéria Magmatic Arc (e.g., Fetter et al., 2003; Costa et al., 2013); 5) Neoproterozoic to Ordovician post-collisional to anorogenic granitoids (Fetter, 1999; Castro et al., 2012).

The Ceará Complex high-grade supracrustal sequences are represented by metamorphic rocks of terrigenous origin (pelites, semi-pelites and greywackes), which are migmatized in some places, and are exposed on both flanks of the Santa Quitéria Magmatic Arc. Quartzite lenses, marbles, calc-silicate rocks, basaltic flows and/or mafic tuffs also occur (Arthaud, 2008). Retroeclogite and high-pressure granulite occurrences associated with these metasedimentary rocks are also recorded on both sides of the Santa Quitéria Magmatic Arc (Castro, 2004; Santos et al., 2009; Amaral et al., 2011, 2012).

The Novo Oriente Group is located in the southwestern portion of the Ceará Central Domain (DCC), more precisely in the Acaraú sub-domain, which is limited by the Transbrasiliano Lineament and the Tauá Shear Zone. The Acaraú sub-domain is characterized by tangential tectonics, with low- to medium-angle foliations dipping NW and subordinately SW. Differently from the other DCC rocks, the Acaraú sub-domain rocks are characterized by low- to medium-grade metamorphism, no anatexis, and still-preserved primary features (Ganade de Araújo et al., 2010, 2011).

The Novo Oriente Group is formed of two distinct tectonic-stratigraphic sequences, related to its sedimentary filling (Cavalcante et al., 2003): the Bonsucesso Formation composed of clastic psamitic deposits, and the Caraúbas Formation, which is dominantly pelitic, with chemical sedimentary contribution (Fig. 2). The occurrence of igneous rocks is at most 15% of the sequence and is marked by the intercalation of metamafic-metaultramafic rocks.

In the northeastern portion, where rocks from the Caraúbas Formation crop out (Fig. 2), the main rock types include: 1) micaceous schists with garnet ± staurolite ± sillimanite ± kyanite ± cordierite porphyroblasts, with highly variable contents of quartz and feldspars, which can develop subordinate thin quartzite layers; 2) phyllites and fine-grained metasandstones with or without biotite; 3) metalimestones; 4) metamafic and metaultramafic rocks; 5) acid flows, pyroclastic layers and volcaniclastic deposits.

In the southwestern portion, micaceous quartzites of the Bonsucesso Formation occur, showing locally conglomeratic sections, interlayered with metamafic rocks and banded iron formations. Regular cm- to m-thick bedding and locally small- to medium-scale oblique stratification represent primary structures of the quartzose sandstone (Ganade de Araújo et al., 2010).

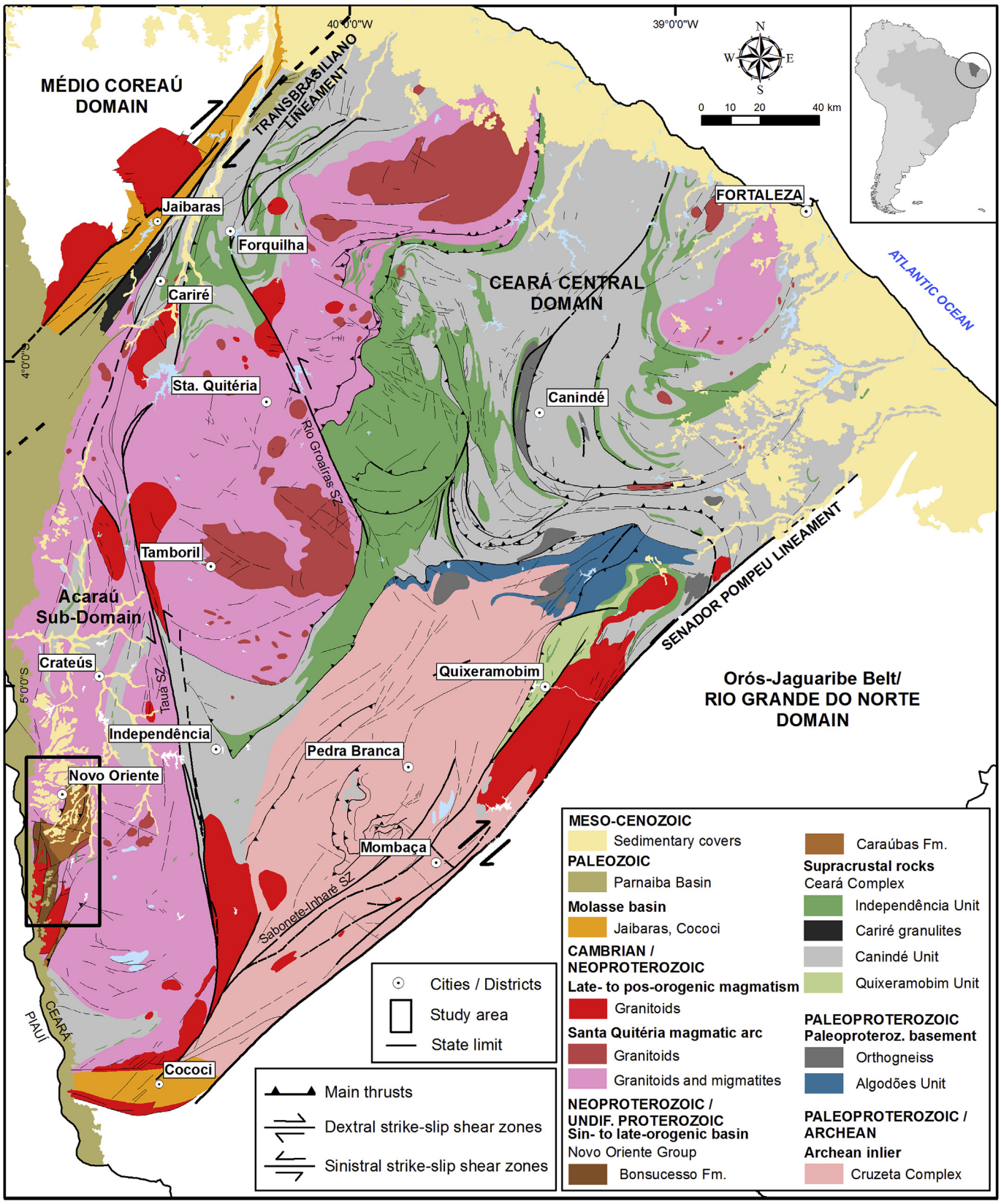

Fig. 1. Simplified geologic map of the Central Ceará Domain (modified after Cavalcante et al., 2003). In detail (black square), Fig. 2.

3. Field occurrence and petrography

The main record of ultramafic rocks is associated with a tectonic sliver preserved in a topographic hill known as Morro dos Pereiras (Fig. 2; Fig. 3A). Metapelitic rocks of low metamorphic grade, encompassed in the metapelitic sequence and comprising phyllites,

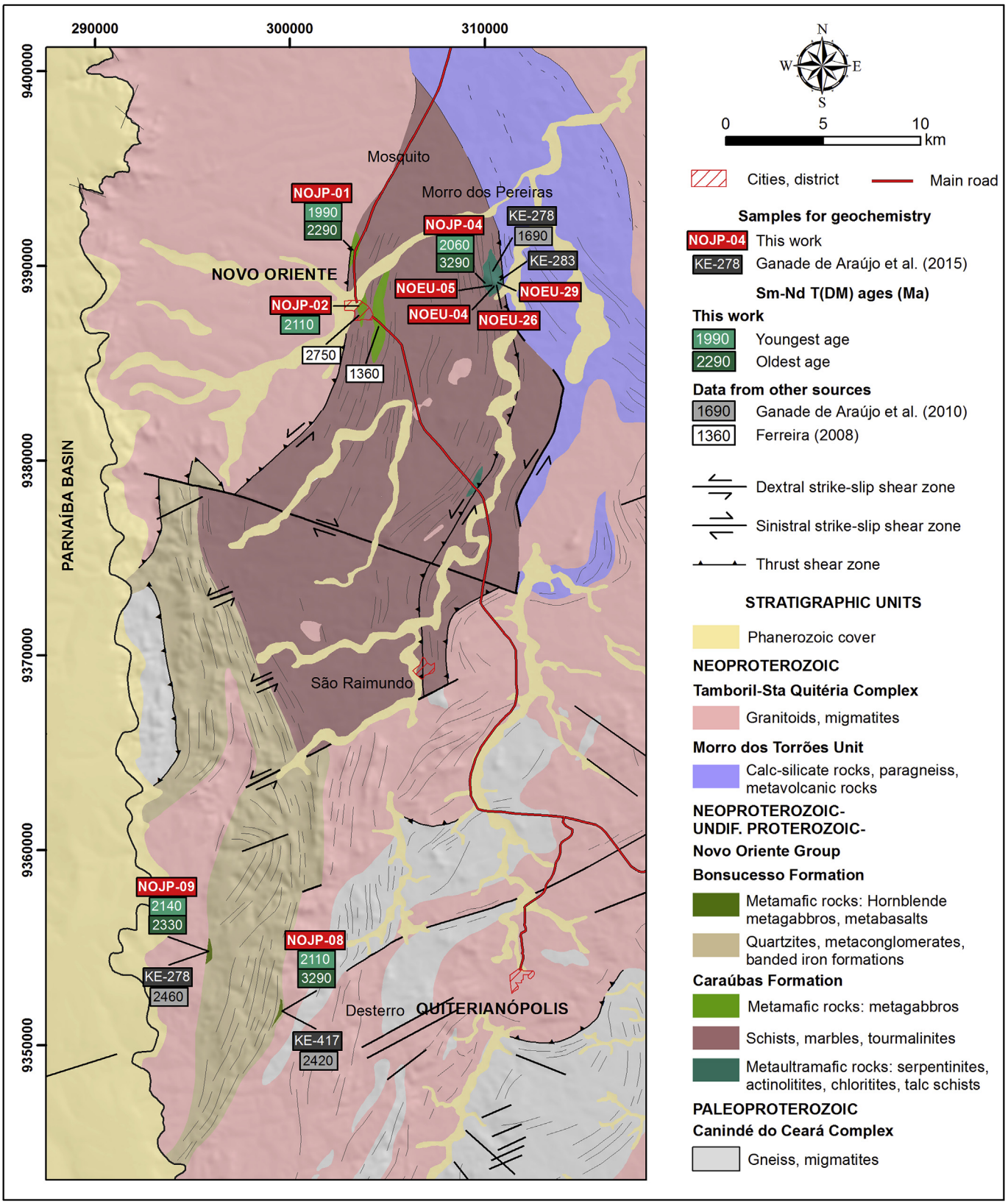

Fig. 2. Regional geological map from the Novo Oriente area showing the main occurrences of metaultramafic and metamafic rocks, isotopic data and location of sampling (adapted from Ganade de Araújo et al., 2011).

schists and kyanitites, dominate the geology of the hill and surroundings. This sequence is in tectonic contact with associations of metaultramafic, meta-exhalative and calc-silicate rocks. The meta-exhalative sequence is constituted of tourmalinites that generally

occur as blocks, which are sometimes in situ. These rocks present rhythmic banding typical of exhalites, with alternating bands of recrystallized quartz (metachert) and bands of tourmaline. Granitoids correlated with the Santa Quitéria magmatic arc (Ganade de Araújo et al., 2012) and metakeratophyres affected by intense metasomatism are also exposed. Cenozoic alluvial and colluvial deposits cover parts of the area.

The structural configuration of the region is marked by planar structures dipping at low angles to SE and linear down-dip structures, associated with low-angle tangential tectonics that gradually turns into transcurrent-transpressional zones, where the planar structures show strong westward dips, and sub-horizontal stretching lineations dipping northward. The dominant metamorphic grade is low to medium-T amphibolite facies in the metapelitic, metaexhalative and the calc-silicate sequences. In the metaultramafic sequence the dominant metamorphic grade is of greenschist facies indicating retrometamorphism. However, presence of Cr-spinel relicts is evidence of previous amphibolite facies conditions.

The rocks belonging to the metaultramafic sequence of Morro dos Pereiras correspond dominantly to sheared or isotropic serpentinites, occurring either in situ or as displaced blocks. The sheared serpentinites are characteristically green to purple and are essentially composed of usually stretched serpentine and Cr-magnetite. The isotropic serpentinites are greenish, massive-textured and composed of serpentine, Cr-magnetite and crosscut by late quartz veins.

The sheared serpentinites are foliated, with stretched serpentine group minerals that imprint a lepidoblastic texture to the rock (Table 1). Shearing is also evidenced by the stretching of Cr-magnetite crystals, revealing an extremely high deformation temperature, probably under mantle conditions. Besides the lepidoblastic texture, mesh-type texture also occurs, characterized by cores of altered olivine relicts rimmed by α-type serpentine, typical of dunite and peridotite serpentinization (Fig. 3B).

Subordinate actinolitites (Fig. 3D), talc-chlorite schists, serpentine-talc schists, chloritites, and talc-rich siliceous rocks

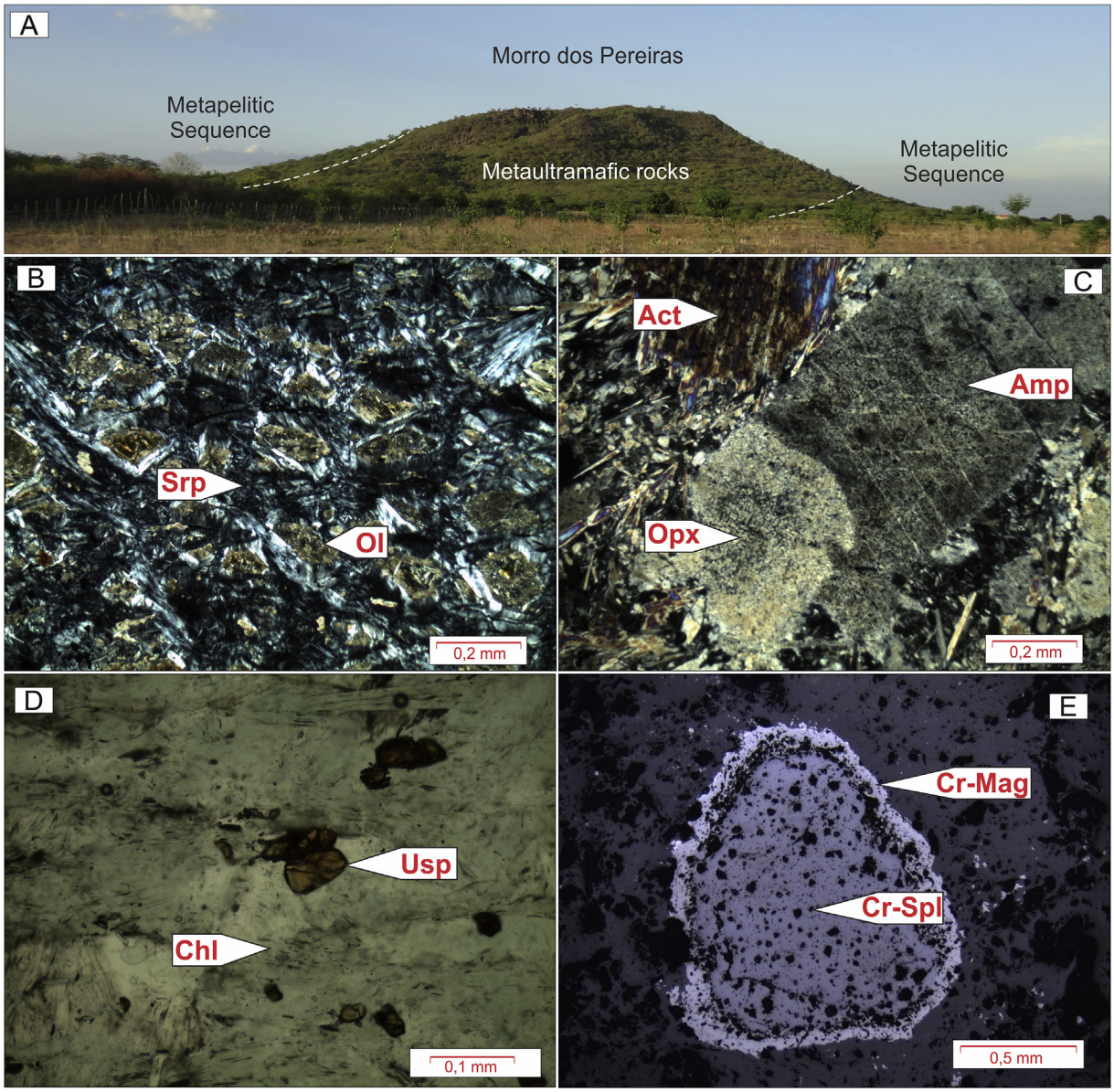

Fig. 3. A) Morro dos Pereiras; B) Serpentinite presenting mesh-type texture; C) orthopyroxene (Opx) higly replace to amphibole (Amp); D) Chloritite presenting ulvöspinel (Usp) crystals inserted in a matrix composed of chlorite (Chl); E) Cr-spinel (Cr-Spl) rimmed by Cr-magnetite (Cr-Mag) in listwänite.

occur as lenticular bodies associated with the serpentinites. Talc-chlorite schists, talc-rich siliceous rocks and serpentine-talc schists frequently occur as blocks, which are sometimes in situ.

The actinolitites present porphyritic texture marked by relict orthopyroxene largely replaced by amphibole (Table 1; Fig. 3E). The mineral assembly is composed of actinolite (50%), hornblende (20%), chlorite (10%), orthopyroxene (10%), serpentine (5%), opaque minerals (3–4%) and Cr-spinel (2-1%).

The talc schists present lepidoblastic and rarely decussate texture (Table 1). Chlorite (clinochlore) is folded and arranged in kink bands, with hinges filled by talc. The mineral assemblage corresponds to clinochlore (65%), talc (30%) and serpentine (5%).

The chloritites present a well-marked foliation and lepidoblastic texture imprinted by chlorite crystals (Table 1; Fig. 3D). The mineral assembly is basically composed of chlorite (85%), ulvöspinel (10%), opaque minerals (5%), and rare biotite.

A typical feature of the metaultramafic sequence is the occurrence of a vein like, hydrothermal alteration cover (listwänites), composed essentially of silica, iron oxides/hydroxides and relict magmatic Cr-spinel crystals rimmed by Cr-magnetite (Fig. 3H–I).

The tourmalinites are characterized by banding typically originated by syngenetic processes in which tourmaline-rich bands alternate with quartz-rich bands. The rock texture is nematoblastic, defined by tourmaline and quartz. The mineral assemblage is composed of tourmaline (60%), quartz (35%), rutile (3%) and opaque minerals (2%).

Metakeratophyres correspond to albitized extrusive felsic rocks, essentially consisting of albite and alteration minerals, such as biotite and carbonates. The rock presents allotriomorphic texture, where almost all minerals are xenoblastic. The mineral assemblage is characterized by albite (50%), dolomite (40%), rutile (5%), opaque minerals (3%) and rare biotite (2%). Spherulitic texture is common.

The metamafic rocks of the Novo Oriente Group occur interspersed both in the metapelitic sequence (Caraúbas Formation) and metapsamitic sequence (Bonsucesso Formation) – (Fig. 1). In Novo Oriente and surroundings, they form concordant lenses accompanying the regional N-S trend (Fig. 4A). They are a few tens of meters wide and between 1 and 4 km long, extending to the colluvial sediments. The out crops are metric size and sometimes accompanied by centimetric and metric blocks usually aligned according to the main orientation of the area (Fig. 4A). North of Novo Oriente, in the Mosquito locality, the metamafic rocks crop out interspersed in metasedimentary rocks of the Caraúbas Formation near the contact with the granitic rocks of the Tamboril-Santa Quitéria Complex (Ganade de Araújo et al., 2012).

Metamafic rocks also occur nearby Desterro in the area of Quiterianópolis municipality, about 35 km to the south of Novo Oriente (Fig. 2). In that area, the metamafic rocks crop out preferably on the edges of the meta-clastic-psamitic sequence of Bonsucesso Formation (Fig. 4B).

The mineralogical variation allowed a preliminary field classification into three metamafic rock groups, which is also confirmed by petrographic studies: metagabbros, hornblende metagabbros and metabasalts.

Metagabbros are of greenish gray color, dominantly isotropic and medium-grained, locally coarse-grained. Concordant to subconcordant mm- to cm-wide felsic veins are common. Asymmetric folds and stratified aspect (primary structures?) occur in portions with more changed gabbroic aspect, with reddish soil and limonite crust associated (Fig. 4C).

The metagabbros are composed of clinopyroxene (30 vol%), hornblende (35%), plagioclase (20%), tremolite-actinolite (9%), and quartz (5%) – Table 1. Titanite, epidote, apatite, opaque, zircon, and baddeleyite are accessory minerals. They present granonematoblastic texture, frequent alteration of clinopyroxene to amphibole, and recrystallization of plagioclase and amphibole (Fig. 4D).

The clinopyroxene is represented by porphyroblast xenomorphs often altered to amphibole featuring uralitization process. Plagioclase occurs in both xenoblastic form and idiomorphic aggregates, sometimes twinned (Carlsbad and polysynthetic). Amphibole commonly replaces porphyroblasts of clinopyroxene up to more than 90%. Some granoblastic aggregates of hornblende and prismatic tremolite-actinolite are also observed. Titanite occurs in xenomorphic form often bordering opaque minerals (ilmenite).

The hornblende metagabbros crop out as centimeter-sized blocks spread over the surface, characteristically associated with red soil (Table 1; Fig. 4E). They present grano-nematoblastic texture, marked by incipient foliation and intense recrystallization of plagioclase and amphibole (Fig. 4F). The main mineralogical association is represented by hornblende (50%), plagioclase (40%), titanite (5%), and opaque minerals (4%). The accessory minerals observed are epidote, apatite and zircon.

Hornblende occurs in green and brown colors (predominance of the first); crystals are xenoblastic and sub-idioblastic prisms. Some crystals are poikilitic, with plagioclase inclusions. Plagioclase occurs in granoblastic aggregates or often as saussuritized xenoblastic crystals. Titanite occurs as xenomorphic crystals and bordering opaque minerals.

The metabasalts, represented by fine-grained amphibolites, crop out as tabular, concordant bodies, interspersed in the eastern

Table 1
Petrography, structure and field characteristics of the rock groups of the study area.

Rock group		Mineralogy		Texture	Structure	Associated rocks
		Essentials	Accessories			
Metamafic rocks	Metabasalts	hbl, pl, qz, ttn	op, ap, zrn	nematoblastic	foliated	meta-clastic-psamitic
	Hornblende metagabbros	hbl, pl	ttn, op, ep, ap, zrn	grano-nematoblastic	isotropic	rocks
	Metagabbros	cpx, hbl, pl, tr-act, qz	ttn, ep, ap, op, zrn, bdy	grano-nematoblastic	isotropic, foliated (locally)	metapelitic rocks
Meta-ultramafic rocks	Chloritites	chl	usp, op, bt	lepidoblastic	schistosity	metapelitic rocks
	Talc schists	clc, tlc	srp	lepidoblastic, decussate	schistosity	
	Actinolitites	act, hbl, chl, opx	srp, op, cr-spl	porphyritic, lepidoblastic	schistosity	
	Sheared serpentinites	srp, ol	cr-mag	mesh-type, lepidoblastic	foliated	
	Isotropic serpentinites	srp	cr-mag	massive	isotropic	

Mineral abbreviations: act: actinolite; ap: apatite; bdy: baddeleyite; bt: biotite; chl: chlorite; clc: clinochlore; cpx: clinopyroxene; cr-mag: cr-magnetite; cr-spl: cr-spinel; ep: epidote; hbl: hornblende; ol: olivine; op: opaque mineral; opx: orthopyroxene; pl: plagioclase; qz: quartz; srp: serpentine; tlc: talc; tr: tremolite; ttn: titanite; usp: ulvöspinel; zrn: zircon.

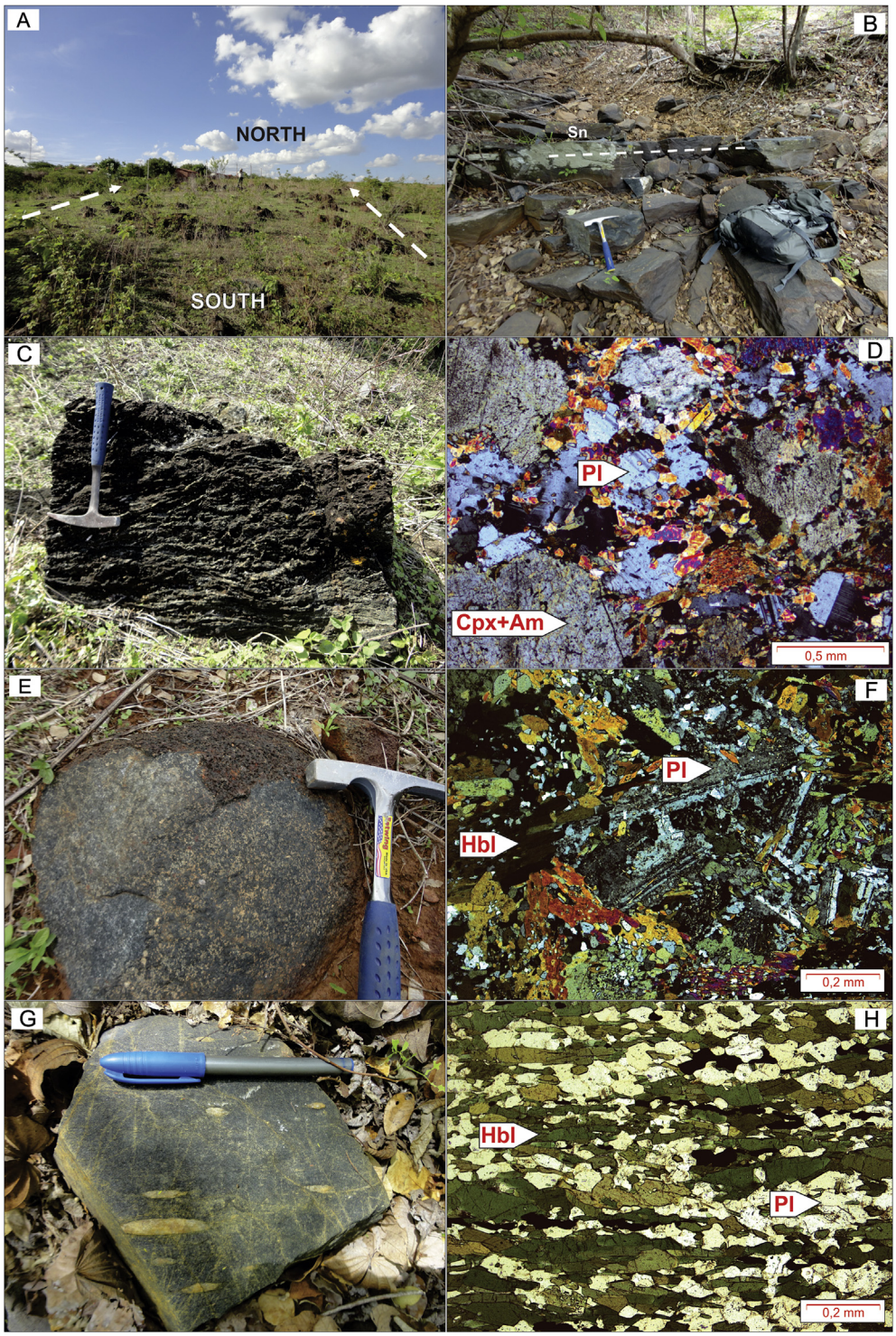

Fig. 4. A) Blocks of metamafic rocks aligned to the main N-S orientation. B) Tabular and concordant outcrops of the metabasalts; C) Stratified aspect (primary structures?) in metagabbro; D) Granonematoblastic texture and frequent alteration of clinopyroxene (Cpx) to amphibole (Am); E) Block of hornblende metagabbro; F) Granonematoblastic texture and intense recrystallization of plagioclase (Pl) and amphibole in hornblende metagabbro; G) Ellipsoidal concentrations oriented by the printed lineation in metabasalt; H) Nematoblastic texture defined by oriented crystals of hornblende and plagioclase.

portion of the quartzite package (Table 1; Fig. 4B). They are of dark green color, and may be oriented or massive. Locally, they display oriented ellipsoidal concentrations of quartz and sometimes feldspar (Fig. 4G). Such features resemble deformed amygdules that indicate the top of the basaltic flows. Cm-sized blocks spread over the surface often exhibit typical spheroidal exfoliation.

The oriented metabasalts are characterized by nematoblastic texture defined by oriented crystals of amphibole (Fig. 4H). The mineral assembly is composed of hornblende (45%), plagioclase (35%), quartz (7%), titanite (7%), and opaque minerals (5%). Apatite and zircon occur in proportions less than 1%. Hornblende is sub idiomorphic, sometimes prismatic, and defines the stretching

lineation. Plagioclase is also oriented; it is saussuritized and sometimes twinned (Carlsbad and/or polysynthetic). Titanite and opaque minerals occur aligned with the minerals that compose the matrix of the rock (Fig. 4H).

Massive metabasalts are isotropic rocks with dark green to black color. They present grano-nematoblastic, medium- to fine-grained equigranular texture. The mineral assemblage is defined by hornblende (50%), plagioclase (30%), tremolite-actinolite (10%), titanite (5%), and quartz (4%). Opaque minerals, apatite, epidote and zircon are accessory. Hornblende is xenoblastic, sometimes subidioblastic and of green or brown color. Plagioclase is xenoblastic, forming the rock matrix with amphibole, or constitutes granoblastic aggregates. The first are usually saussuritized while the latter are characterized by clear crystals without twinning.

4. Geochemistry

Whole-rock chemical analyses were carried out at Acme Analytical Laboratories LTD., Vancouver, Canada, adopting Group 4A and 4B packages. In the first, the weight percentages of major oxides and several trace elements were obtained from 0.2 g of sample analyzed by inductively coupled plasma – emission spectroscopy (ICP-ES). In the second, the contents of rare earth and refractory elements were obtained from 0.2 g of sample by inductively coupled plasma–mass spectrometry (ICP-MS).

Twenty-nine samples of metaultramafic and metamafic rocks were analyzed. The data were treated using *GCDKIT tools* (Version 3.0) and *Microsoft Excel* 2007. The results for major, trace and rare-earth elements are listed in Tables 2 and 3.

The analyzed samples were highly modified by deformation and metamorphism under greenschist and amphibolite facies conditions. The elements used in this work are those used by Furnes et al. (2015) and Pearce (2014), given that their concentrations are usually little affected by alteration processes. We used compatible elements (Cr, Ni, Co, Al and V) and High Field Strength Elements (Zr, Ti, Th, Ta, Nb and Y) to build variation diagrams. Rare Earth Elements (REE) and incompatible elements were normalized in relation to primitive mantle composition. For metamafic rocks, we also used rock classification diagrams, magmatic series, and discrimination of tectonic environments.

4.1. Metaultramafic rocks

4.1.1. Variation diagrams

The serpentinites correspond to rocks that represent the most primitive magma, due to their high Cr and Ni contents, ranging from 2300 to 2900 ppm, and 2165–2660 ppm, respectively (Fig. 5A). They present the lowest Al (960–1350 ppm) and V (between 8 and 30 ppm) contents, whereas Co contents vary between 105 and 111 ppm. Regarding HFSE, the serpentinites present very low Zr (0.1–0.8 ppm), Ti (average 60 ppm), Nb (0.03–0.1 ppm), Ta (0.1 ppm), and Y (0.2–0.5 ppm) contents – Fig. 5E, F, I, J.

The actinolitites tend to present a more differentiated composition than the serpentinites with high Cr and Ni contents, respectively 1500–3187 ppm and 375–1200 ppm (Fig. 5). They present intermediate Al contents, ranging between 1600 and 3200 ppm. They correspond to rocks with low Co concentrations, ranging between 40 and 75 ppm. On the other hand, they tend to present the largest V contents, between 125 and 165 ppm. Regarding HFSE, these rocks present intermediate Ti contents, ranging between 1740 and 2700 ppm. Similar to Ti, Zr (12.5–78 ppm), Nb (0.5–6.8 ppm), Ta (0.1–0.4 ppm), and Y (11.1–22 ppm) present intermediate concentrations.

Talc schist is characterized by low Cr content (35 ppm). Ni content is lower than in serpentinite and actinolitites (Fig. 5). Al content (3700 ppm) is similar to those in actinolitites. The concentration of Co and V is similar to those in the serpentinite, reaching 105 ppm and 8 ppm, respectively. As for HFSE, talc schist presents Ti content of 230 ppm and intermediate Zr, Nb, Ta and Y contents, reaching 87 ppm, 10.8 ppm, 1.4 ppm and 10 ppm, respectively.

The chloritites correspond to rocks with the lowest Cr contents (27–60 ppm) – Fig. 5. Ni content is intermediate, reaching 900 ppm. Al and Co contents are high, 5400–5700 ppm and 134–135 ppm, respectively, when compared to those of other rocks. The chloritites present intermediate V contents, ranging between 104 and 135 ppm. Regarding HFSE, these are the rocks that present the highest Ti (10,000–15,000 ppm), Zr (170–240 ppm), Nb (15–18 ppm), and Ta (0.9 ppm) contents. Y contents are variable.

The binary variation diagrams with Zr in the abscissae show the degree of differentiation in the studied rocks. It can be seen that Co and Al contents tend to increase as the concentration of Zr increases (Fig. 5). The V concentrations present variable behavior, but they increase in its concentration as Zr of actinolitites increases toward the chloritites. Similarly to Al and Co, the HFSE tend to increase their concentrations as Zr increases.

4.1.2. Spidergrams

Samples of metaultramafic rocks were normalized to the primitive mantle (Sun and McDonough, 1989). Spidergrams of serpentinite include samples of Deschamps et al. (2013) comprising subducted serpentinites originated through alteration of dunites (Fig. 6A and B). The average compositions of the mafic lower crust (Rudnick and Gao, 2003) and E- and N-MORB (Sun and McDonough, 1989) were also plotted in the diagrams for actinolitites and talc schists for comparison (Fig. 6C–H).

The serpentinites are ten times more depleted in Rare Earth Elements (REE) than the primitive mantle (Fig. 6A). They are rich in La, somewhat depleted in Ce, and display relatively flat distribution toward HREE. They present slight enrichment of Cs, Ba, Th, U, Ta, Pb, and P, and depletion of Rb, Nb, Ce, Pr, Sr, Zr, Ti and Y (Fig. 6A). When compared to the average composition of serpentinites presented by Deschamps et al. (2013), the Morro do Pereira serpentinites resemble sub-continental mantle peridotites, exhumed and hydrated during rifting in OCT (*ocean-continental transition*), appearing to be the result of dunite alteration (Fig. 6A–B).

The actinolitites are rich in REE when compared to primitive mantle, and slightly depleted in Ce with a relatively flat distribution from LREE to HREE (Fig. 6C). They are enriched in incompatible elements when compared to primitive mantle, and characterized by strong enrichment in Cs, Th, U, La, Ce, Nd, and Sm, as well as depleted in Rb, Nb, Pb, Sr, Zr, and Eu. In addition, the actinolitites present a REE distribution similar to the average composition of the lower crust and E-MORB (Fig. 6D).

The chloritites are ten to one hundred times more enriched than the primitive mantle (Fig. 6E). They are rich in LREE and depleted towards HREE with slight negative anomalies in Ce and Eu. They are enriched in incompatible elements when related to the primitive mantle, displaying positive anomalies in Cs, Ba, Th, U, Nb, Ta, La, Ce, Pr, and Nd, as well as strong negative anomalies of Rb, Pb and Sr (Fig. 6F).

The two talc schist samples analyzed have different patterns. The NOEU-26D sample shows a relatively flat REE pattern and is up to 10 times enriched when compared to the primitive mantle. This sample presents a negative Eu anomaly and shows similarities to the average distribution of trace elements in the lower mafic crust and E-MORB (Fig. 6G). The NOEU-29B sample presents REE depletion and slight LREE enrichment, and positive Eu anomaly, similar to serpentinized dunites involved in subduction (Fig. 6G). Cs, Ba, Th, U, Nb, Ta, La, Pb, P, and Nd enrichment, as well as strong

Table 2
Major (wt%), trace and rare earth elements (ppm) analyses for the metaultramafic rocks of the Novo Oriente region. CHL: chloritite; ACT: actinolitite; SP: serpentinite; TCS: talc schist. *Samples from Ganade de Araújo and Pinéo (2015).

Sample	NOJP-04C	NOEU-04B	NOEU-05	*KE-283	NOJP-04D	NOEU-04A	*KE-278
Rock	SP	SP	SP	SP	ACT	ACT	ACT
UTM Coordintates	9388999/310211	9388909/310502	9388934/310386	9388940/310666	9388999/310211	9388909/310502	9389744/310404
Major elements (%)							
SiO_2	39.46	39.49	40.60	36.68	48.20	50.13	48.41
TiO_2	0.01	0.01	0.01	0.01	0.29	0.45	0.75
Al_2O_3	0.46	0.45	0.38	0.37	7.59	6.09	12.16
Fe_2O_3	8.59	7.36	8.23	7.01	10.37	8.35	9.52
MgO	36.19	36.69	36.54	38.64	19.47	20.21	13.53
CaO	0.03	0.10	0.02	0.03	9.02	9.70	12.89
Na_2O	0.01	0.01	0.01	0.01	0.40	0.30	0.79
MnO	0.09	0.09	0.05	0.08	0.19	0.2	0.29
P_2O_5	0.02	0.02	0.01	0.03	0.03	0.03	0.14
LOI	13.80	14.50	12.80	15.9	3.80	3.90	0.8
Total	98.66	98.61	98.58	98.77	99.36	99.18	99.58
Trace elements (ppm)							
Cr	2901	2463	2935	2326	1266	821	616
Ni	2659	2555	2467	2163	753	1201	375
Co	105.60	109.70	111.00	111.30	73.20	57.70	41.00
Ba	10.00	13.00	20.00	6.00	5.00	7.00	28.00
Sr	1.50	1.60	1.30	1.70	6.80	8.80	53.40
Zr	0.80	0.60	0.60	0.10	13.00	12.50	78.20
Nb	0.10	0.10	0.10	0.03	1.00	0.50	6.80
Y	0.30	0.50	0.20	0.20	13.00	11.10	22.00
V	12.00	8.00	8.00	30.00	123.00	126.00	165.00
La	0.30	0.20	0.20	0.30	3.00	2.40	12.30
Ce	0.20	0.20	0.10	0.30	5.00	3.70	25.30
Pr	0.02	0.02	0.02	0.03	0.99	0.78	3.82
Nd	0.30	0.30	0.30	0.30	5.00	3.90	15.20
Sm	0.05	0.05	0.05	0.05	1.31	1.24	3.51
Eu	0.02	0.02	0.02	0.02	0.64	0.40	1.12
Gd	0.05	0.05	0.05		1.68	1.68	3.93
Tb	0.01	0.01	0.01	0.01	0.33	0.30	0.67
Dy	0.05	0.07	0.05	0.05	2.45	2.04	3.72
Ho	0.02	0.02	0.02	0.02	0.49	0.37	0.82
Er	0.05	0.06	0.03	0.03	1.33	1.14	2.11
Tm	0.01	0.01	0.01	0.01	0.21	0.20	0.36
Yb	0.05	0.05	0.05	0.05	1.30	1.17	2.24
Lu	0.01	0.01	0.01	0.01	0.17	0.17	0.34
Cs	0.10	0.10	0.10	0.10	0.10	0.10	1.70
Rb	0.10	0.10	0.10	0.40	0.10	0.60	9.50
Th	0.20	0.20	0.20	0.20	0.20	0.20	3.10
U	0.10	0.10	0.10	0.10	0.10	0.10	0.70
Ta	0.10	0.10	0.10	0.10	0.10	0.10	0.40
Pb	0.30	0.60	0.10		0.10	0.10	

Sample	NOJP-04A	NOJP-04B	NOEU-26D	NOEU-29B
Rock	CHL	CHL	TCX	TCX
Coordintates Lat/Long	9388999/310211	9388999/310211	9389237/310384	9389202/310494
Major elements (%)				
SiO_2	29.49	27.88	38.17	41.7
TiO_2	1.65	2.51	0.04	0.01
Al_2O_3	20.93	21.95	14.13	0.53
Fe_2O_3	5.73	6.86	3.75	6.87
MgO	29.16	27.57	31.25	35.65
CaO	0.03	0.45	0.01	0.02
Na_2O	0.01	0.01	0.01	0.01
MnO	0.04	0.04	0.02	0.06
P_2O_5	0.10	0.33	0.01	0.02
LOI	12.10	11.70	12	13.9
Total	99.24	99.30	99.34	98.69
Trace elements (ppm)				
Cr	27	62	34	2306
Ni	1146	1543	911	2294
Co	134.30	135.80	105.5	55.2
Ba	244.00	21.00	5	15
Sr	62.40	8.90	0.6	1.7
Zr	169.60	240.20	87.8	0.4
Nb	18.00	15.60	10.8	0.1
Y	34.60	6.70	10.4	0.3
V	104.00	131.00	8	8
La	57.20	10.50	5.5	0.5

Table 2 (*continued*)

Sample	NOJP-04A	NOJP-04B	NOEU-26D	NOEU-29B
Rock	CHL	CHL	TCX	TCX
Coordintates Lat/Long	9388999/310211	9388999/310211	9389237/310384	9389202/310494
Ce	62.30	16.10	10.3	0.1
Pr	12.75	2.64	1.05	0.02
Nd	54.10	9.70	3.9	0.3
Sm	10.90	2.21	0.8	0.05
Eu	3.04	0.48	0.08	0.02
Gd	10.00	1.81	1.07	0.05
Tb	1.48	0.25	0.27	0.01
Dy	8.52	1.39	2.06	0.05
Ho	1.38	0.22	0.49	0.02
Er	3.31	0.51	1.39	0.03
Tm	0.43	0.08	0.21	0.01
Yb	2.29	0.55	1.41	0.05
Lu	0.30	0.06	0.12	0.01
Cs	0.10	0.10	0.1	0.1
Rb	0.10	0.10	0.1	0.1
Th	8.30	0.40	9.7	0.2
U	3.40	1.10	0.7	0.1
Ta	0.80	0.90	1.4	0.1
Pb	0.10	0.10	0.3	0.1

negative Rb, Nb, Ce, Pr, Sr, Zr, and Ti anomalies are also observed (Fig. 6H).

4.2. Metamafic rocks

4.2.1. Variation diagrams

The metagabbros correspond to the earliest mafic terms with Cr and Ni contents ranging from 190 to 590 ppm, and from 80 to 230 ppm, respectively (Fig. 7A). They present the lowest Al (199532-60280 ppm), and V contents (285-140 ppm), whereas Co, Zr and Y are variable (Fig. 7B, D and J). Regarding HFSE, the metagabbros present the lowest Ti (11,992–5996 ppm), Th (1.3–2.6 ppm), Ta (0.2–0.4 ppm) and Nb (1.7–3.6 ppm) contents (Fig. 7F–I). In several diagrams the samples are scattered and show a distinct geochemical behavior compared to the other two groups (Fig. 7 – Al x Cr; V x Cr; Zr x Cr; Y x Cr; Al x Zr), suggesting that genetic relationships between the sources are unlikely.

The hornblende metagabbros are an intermediate term between the two other groups of metamafic rocks, tending closer to metabasalts (Fig. 7) as suggested by HFSE elements (Zr, Ti, Th, Ta, and Nb). They have different values of Co (43.8–74.7 ppm) and lower Y (17.6–20.9 ppm) – Fig. 7.

The metabasalts differ from the other groups. They are characterized by lower values of compatible elements Ni (46–75 ppm) and Cr (61.6–109.5 ppm) – Fig. 7A, and they display the highest HFSE contents. Their Al (61,816.5–78,646.7 ppm) and V (186–304 ppm) contents are similar to those of the hornblende metagabbro group (Fig. 7).

4.2.2. Geochemistry of immobile elements, rock classification diagrams, and magmatic series

Pearce (2014) showed that Ti and Zr, both considered immobile elements, correlate in MORB-type suites (Fig. 8A). When Ti is replaced by the mobile element K, fresh unweathered samples continue to show significant correlation. However, they show enrichment in weathered and in amphibolite facies samples, in contrast to depletion in samples of rocks that underwent greenschist facies conditions. In the Ti x Zr diagram for metamafic rocks from Novo Oriente, the samples present good correlation, and values ranging from the trend of unaltered rocks to greenschist facies metamorphic types (Fig. 8A). Similar behavior is observed when replacing Ti by K, considered to be a mobile element (Fig. 8B). It suggests that the samples analyzed in this study were little affected by alteration processes, although alteration features were observed in thin sections, such as saussuritization and uralitization.

Fresh rocks are usually classified by the total alkali-silica diagram (TAS, Le Bas and Streckeisen, 1991) as recommended by the IUGS. According to Pearce (2014), the elements of this diagram (K, Na and Si) are highly mobile, proposing instead the use of the Nb/Y vs. Zr/Ti diagram (Pearce, 1996) as the most suitable to classify altered or slightly altered rocks. In this diagram, the hornblende metagabbro group and the metabasalts plot in the basalt field whereas the metagabbros have lower Nb/Y ratios and tend to the field of basaltic andesites.

The tholeiitic character of metamafic rocks from Novo Oriente is displayed in the AFM diagram (Irvine and Baragar, 1971). The diagram clearly shows the iron enrichment from metagabbros to metabasalts (Fig. 8D). In the Jensen (1976) diagram (Fig. 8E), analyzed samples plot in the field of high-Fe tholeiitic basalts (metabasalts and hornblende metagabbros) and of komatiitic basalts (metagabbros). Metagabbro sample NOJP-01C is classified as high-Mg tholeiitic basalt.

4.2.3. Spidergrams

The distribution of Rare Earth Elements (REE) normalized by the primitive mantle, and compared to the patterns of the mafic lower crust, E- and N-MORB are shown in Fig. 9. The samples present a similar arrangement, and a very fractionated pattern marked by the enrichment of light REE and depletion of heavy REE (Fig. 9A–C). In the La-Sm segment, they present enrichment of up to 10^2 times compared to primitive mantle, and feature a parallel pattern to the lower crust and E-MORB. The heavy REEs present a relatively flat to depleted pattern, similar to the lower crust (Fig. 9A–C). The La/Yb_N ratios vary between 3.65 and 17.13. The lowest values are observed in samples from the metabasalt group while the highest values are in the metagabbros (Fig. 9A). A similar pattern is observed in the Ce/YbN ratio (3.33–14.78).

The multi-element diagrams show the behavior of metamafic rocks relative to primitive mantle, also compared to mafic lower crust patterns (Rudnik and Gao, 2003), E-MORB and N-MORB (Sun and McDonough, 1989). In general, the samples present an enriched pattern marked by the overlap of the different the groups.

Table 3
Major (wt%), trace and rare earth elements (ppm) analyses for the metamafic rocks of the Novo Oriente region. MG: metagabbro; HMG: hornblende metagabbro; MB: metabasalt. *Samples from Ganade de Araújo and Pinéo (2015).

Sample	NOJP-01A	NOJP-01B	NOJP-01C	NOJP-01D	NOJP-02	NOJP-09A	NOJP-09B
Rock	MG	MG	MG	MG	MG	HMG	HMG
UTM Coordintates	9390052/303300	9390052/303300	9390052/303300	9390052/303300	9390052/303300	9355049/295747	9355049/295747
Major elements (%)							
SiO_2	48.08	46.52	44.65	47.40	49.95	50.89	50.95
TiO_2	1.03	1.60	0.98	0.80	1.05	1.43	1.53
Al_2O_3	6.68	7.58	11.39	8.78	3.77	14.86	14.29
$Fe_2O_3^T$	8.86	12.35	8.93	13.32	9.04	11.97	12.13
MgO	10.88	10.82	8.06	13.09	11.66	6.49	6.65
CaO	20.37	17.70	22.89	13.31	21.06	10.63	11.20
Na_2O	0.98	1.09	0.31	0.85	0.81	1.85	1.49
K2O	0.30	0.58	0.10	0.30	0.41	0.42	0.44
P_2O_5	0.59	0.20	0.63	0.10	0.13	0.13	0.12
LOI	1.50	0.90	1.40	1.30	1.40	0.90	0.80
Total	99.27	99.34	99.34	99.25	99.28	99.57	99.60
Trace elements (ppm)							
Cr	273.68	294.21	191.58	540.52	588.41	82.10	88.95
Ni	82.00	115.00	35.00	230.00	97.00	75.00	73.00
Co	100.20	76.20	52.20	150.10	52.90	62.60	68.40
Ba	119.00	146.00	84.00	77.00	95.00	115.00	103.00
Sr	232.40	190.40	1192.00	142.00	63.40	293.90	255.00
Zr	95.00	177.70	103.20	58.20	126.90	100.50	96.40
Nb	1.90	3.60	2.30	1.70	1.90	5.60	5.80
Y	32.50	25.10	16.00	29.50	20.90	20.20	20.90
V	228.00	285.00	139.00	169.00	173.00	273.00	291.00
La	22.20	27.40	28.70	29.00	11.20	14.90	19.90
Ce	59.30	67.00	64.00	51.90	30.40	32.30	39.50
Pr	9.14	8.86	7.88	8.27	4.81	3.83	4.65
Nd	40.40	36.90	33.10	34.80	22.50	15.80	18.60
Sm	8.67	7.91	5.89	7.18	6.26	3.78	4.26
Eu	1.84	1.78	1.38	1.88	1.39	1.20	1.60
Gd	8.30	7.13	4.85	6.84	5.49	4.04	4.39
Tb	1.20	1.00	0.63	1.00	0.82	0.64	0.72
Dy	6.71	5.48	3.38	5.58	4.18	3.83	4.06
Ho	1.22	0.91	0.58	0.94	0.72	0.77	0.76
Er	3.03	2.52	1.61	2.69	2.14	2.15	2.23
Tm	0.40	0.33	0.20	0.36	0.27	0.29	0.30
Yb	2.28	1.77	1.14	2.19	1.63	1.77	1.77
Lu	0.32	0.26	0.15	0.26	0.20	0.26	0.23
Cs	1.80	0.30	0.70	0.10	2.10	0.30	0.40
Rb	6.50	5.70	4.40	3.70	15.70	5.20	6.30
Th	1.60	2.60	2.40	1.30	1.70	2.50	2.60
U	0.50	0.80	0.80	0.40	1.30	0.60	1.40
Ta	0.30	0.40	0.20	0.20	0.30	0.40	0.50
Pb	6.50	5.40	8.30	1.60	1.60	2.20	3.50
Hf	3.7	5.3	3.3	1.9	4.3	2.9	2.9

Amostra	NOJP-09C	NOJP-09D	*KE-421B	NOJP-08A	NOJP-08B	NOJP-08C	NOJP-08D	NOJP-08E
Rocha	HMG	HMG	HMG	MB	MB	MB	MB	MB
Coordintates Lat/Long	9355049/295747	9355049/295747	9355049/295747	9351967/299556	9351967/299556	9351967/299556	9351967/299556	9351967/299556
Major elements (%)								
SiO_2	50.11	51.08	50.85	50.86	50.39	50.74	49.80	51.14
TiO_2	1.28	1.48	1.46	1.74	1.46	1.54	1.68	1.65
Al_2O_3	15.23	14.48	15.08	14.51	12.39	14.27	13.62	14.55
$Fe_2O_3^T$	12.02	13.01	11.94	12.79	12.50	13.74	13.54	13.04
MgO	7.33	6.32	6.29	5.94	5.00	5.94	6.01	5.59
CaO	10.90	10.45	11.01	8.94	15.11	8.57	12.50	8.74
Na_2O	1.47	1.68	1.66	3.63	1.64	3.32	0.98	3.46
K2O	0.25	0.32	0.49	0.54	0.40	0.64	0.29	0.62
P_2O_5	0.11	0.14	0.13	0.17	0.15	0.15	0.16	0.16
LOI	0.80	0.60	0.7	0.40	0.50	0.70	1.00	0.60
Total	99.50	99.56	99.61	99.52	99.54	99.61	99.58	99.55
Trace elements (ppm)								
Cr	212.10	88.95	68.42	75.26	88.95	95.79	102.63	75.26
Ni	105.00	71.00	59.00	64.00	62.00	73.00	59.00	66.00
Co	74.70	72.20	43.80	69.40	59.30	60.90	52.20	58.70
Ba	36.00	96.00	108.00	145.00	80.00	113.00	51.00	95.00
Sr	355.90	318.20	272.00	309.50	607.20	309.80	682.80	287.30
Zr	91.80	103.80	98.80	141.20	114.30	116.70	117.20	144.30
Nb	6.00	6.60	6.70	9.40	7.00	8.60	8.70	9.40
Y	17.60	20.00	20.70	25.40	21.10	23.10	25.80	27.70
V	248.00	274.00	307.00	304.00	234.00	275.00	285.00	299.00

Table 3 (*continued*)

Amostra	NOJP-09C	NOJP-09D	*KE-421B	NOJP-08A	NOJP-08B	NOJP-08C	NOJP-08D	NOJP-08E
Rocha	HMG	HMG	HMG	MB	MB	MB	MB	MB
Coordintates Lat/Long	9355049/295747	9355049/295747	9355049/295747	9351967/299556	9351967/299556	9351967/299556	9351967/299556	9351967/299556
La	12.50	13.50	13.70	19.90	17.90	10.80	17.90	18.90
Ce	26.40	30.00	28.10	43.10	36.10	27.70	39.10	39.60
Pr	3.19	3.58	3.78	5.27	4.22	3.57	4.81	5.35
Nd	13.90	15.40	15.10	22.20	17.10	18.10	18.80	19.50
Sm	3.09	3.82	3.65	4.91	3.94	4.35	4.83	5.33
Eu	1.10	1.22	1.30	1.51	1.28	1.26	1.69	1.66
Gd	3.48	3.99	3.94	5.58	4.36	4.71	5.74	5.52
Tb	0.57	0.66	0.68	0.84	0.68	0.77	0.75	0.95
Dy	3.18	3.85	3.75	5.17	3.43	4.20	4.60	5.46
Ho	0.69	0.79	0.75	1.00	0.75	0.92	0.80	1.03
Er	1.90	2.21	2.18	2.70	2.24	2.53	2.38	2.77
Tm	0.24	1.05	0.28	0.38	0.30	0.36	0.37	0.39
Yb	1.70	1.69	1.91	2.24	1.83	2.06	2.09	2.20
Lu	0.22	0.22	0.26	0.33	0.25	0.30	0.29	0.32
Cs	0.20	0.30	0.60	0.10	1.00	0.30	0.30	0.20
Rb	2.20	2.40	8.80	7.20	7.00	12.40	1.40	5.50
Th	2.10	2.50	2.30	4.50	3.60	3.60	3.00	4.30
U	0.40	0.40	0.70	0.70	0.70	0.50	0.60	0.90
Ta	0.40	0.60	0.50	0.80	0.50	0.50	0.60	0.60
Pb	2.50	4.90	2.60	0.60	0.40	0.60	1.30	0.60
Hf	2.6	2.8	2.9	3.3	2.9	2.8	3.6	3.5

Amostra	NOJP-08F	NOJP-08G	NOJP-08H	NOJP-08I	NOJP-08J	NOJP-08L	*KE-417
Rocha	MB	MB	MB	MB	MB	MB	MB
Coordintates Lat/Long	9351967/299556	9351967/299556	9351967/299556	9351967/299556	9351967/299556	9351967/299556	9351967/299556
Major elements (%)							
SiO_2	50.98	49.71	52.30	51.34	49.98	50.99	51.9
TiO_2	1.62	1.55	2.07	1.48	1.68	1.80	1.75
Al_2O_3	14.37	13.21	11.68	14.58	14.86	14.36	14.33
$Fe_2O_3^T$	13.38	13.27	12.18	13.28	13.69	12.95	12.72
MgO	6.41	4.15	5.19	5.91	5.97	6.12	5.88
CaO	8.51	14.73	13.24	7.89	8.61	8.46	8.5
Na_2O	3.32	2.07	1.06	3.87	3.63	3.69	3.56
K2O	0.30	0.48	0.75	0.45	0.43	0.44	0.56
P_2O_5	0.15	0.15	0.32	0.14	0.17	0.17	0.19
LOI	0.50	0.20	0.80	0.70	0.60	0.60	0.2
Total	99.54	99.52	99.59	99.64	99.62	99.58	99.59
Trace elements (ppm)							
Cr	88.95	82.10	61.58	109.47	68.42	75.26	68.42
Ni	75.00	46.00	56.00	72.00	56.00	67.00	59.00
Co	66.00	85.60	55.70	74.90	59.50	63.20	44.60
Ba	54.00	95.00	297.00	58.00	55.00	49.00	205.00
Sr	281.80	855.40	343.40	224.50	298.00	424.30	251.60
Zr	128.60	116.70	268.10	117.40	143.90	144.10	139.60
Nb	8.10	7.60	17.10	7.50	8.70	8.70	10.40
Y	26.10	23.20	38.60	25.00	27.30	25.00	26.10
V	294.00	271.00	186.00	296.00	292.00	265.00	302.00
La	13.20	16.80	43.80	12.60	19.00	11.80	18.40
Ce	29.30	36.40	82.80	29.40	42.80	27.80	39.30
Pr	4.24	4.18	9.81	3.87	5.13	4.00	5.32
Nd	20.00	18.10	37.50	17.00	21.10	18.70	21.40
Sm	4.75	4.26	8.24	4.24	5.05	4.65	5.03
Eu	1.46	1.40	2.22	1.59	1.56	1.27	1.38
Gd	4.82	4.69	8.59	5.00	5.23	5.06	4.97
Tb	0.79	0.74	1.33	0.77	0.87	0.81	0.85
Dy	4.92	4.23	7.51	4.41	4.94	4.47	4.56
Ho	0.92	0.92	1.52	0.91	0.99	0.90	0.97
Er	2.63	2.48	4.10	2.50	2.79	2.54	2.80
Tm	0.37	0.31	0.60	0.36	0.40	0.37	0.39
Yb	2.30	2.05	3.91	2.18	2.23	2.20	2.38
Lu	0.30	0.29	0.58	0.30	0.35	0.31	0.35
Cs	0.10	1.60	1.50	0.20	0.10	0.30	0.10
Rb	1.90	4.30	20.80	7.50	3.10	8.70	11.00
Th	4.30	3.20	8.70	3.20	4.60	4.80	4.30
U	0.60	0.80	1.30	0.50	0.70	0.70	0.60
Ta	0.70	0.70	1.00	0.60	0.60	0.70	0.70
Pb	0.40	0.50	0.80	0.50	0.40	0.50	0.80
Hf	3.5	3.3	7	3.5	3.9	4.2	4.1

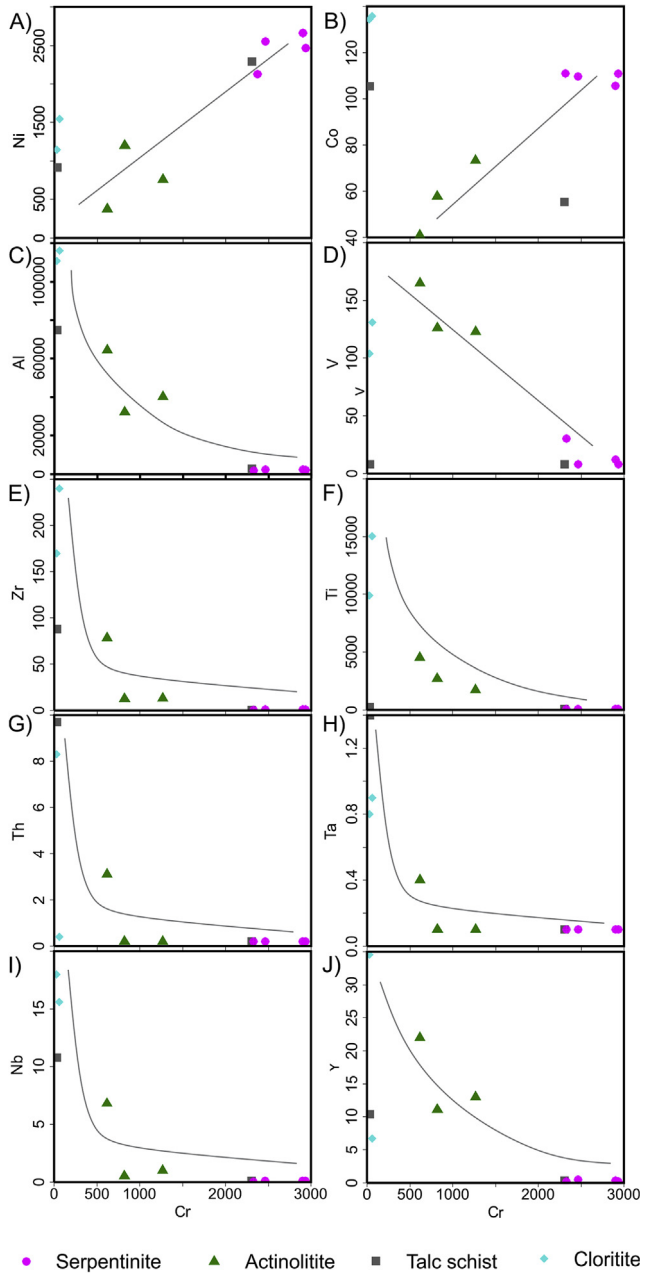

Fig. 5. Variation diagrams for the metaultramafic rocks: A) Ni x Cr; B) Co x Cr; C) Al x Cr; D) V x Cr; E) Zr x Cr; F) Ti x Cr; G) Th x Cr; H) Ta x Cr; I) Nb x Cr; J) Y x Cr.

The metagabbros present a more irregular pattern and stand out due to the negative anomalies of Nb, Sr, and Zr (Fig. 9D). They present positive and negative anomalies of Cs, Pb, and Sr. The group of hornblende metagabbros shows a pattern similar to the metabasalts, differing only in the Pb content, which in this group is marked by positive anomalies (Fig. 9E). The group of metabasalts (Fig. 9F) is characterized by strong negative anomalies of Rb and Pb. Lesser negative anomalies of Nb and P are observed. Positive anomalies are recorded for Cs, Th, La, Sr, and Nd. In general, the two groups follow the pattern defined for E-MORB and mafic lower crust.

4.2.4. Tectonomagmatic discrimination diagrams

In the Ti x V diagram (Shervais, 1982) for metamafic rocks from Novo Oriente, the samples plot in the Ti/V = 20–50 interval of the ocean floor basalts field (Fig. 10A).

In the Zr x Ti diagram (Pearce, 1982), the metabasalts and hornblende metagabbros plot in the intersection between the MORB and intra-plate basalt fields (Fig. 10B). Despite their larger dispersion, metagabbros present a trend parallel to MORB, divided between the island arc and intra-plate fields.

Besides the chemical composition similar to MORB, the samples present an intra-plate basalt composition as shown in the Zr x Zr/Y diagram (Fig. 10C, Pearce and Norry, 1979).

In the triangular Th-Zr-Nb system of Wood (1980) – Fig. 10D, the samples plot in the calc-alkaline basalts field. Although this system does not distinguish between E-MORB and intra-plate basalts, it points to a low probability of an island arc environment for the generation of the analyzed rocks.

5. Nd isotopes

The bulk rock Sm–Nd isotopic analyses were carried out at the Laboratory of Geochronology at University of Brasília. The samples were dissolved in Teflon Savillex beakers or in Parr-type Teflon bombs. Sm and Nd extraction from whole-rock powders and garnet concentrates followed the technique described in Richard et al. (1976) and Gioia and Pimentel (2000), in which the separation of the REE as a group using cation-exchange columns precedes reversed-phase chromatography for the separation of Sm and Nd using columns loaded with HDEHP (di-2-ethylhexyl phosphoric acid) supported on Teflon powder. We also used the RE-Spec and Ln-Spec resins for REE and Sm–Nd separation. A mixed ^{149}Sm–^{150}Nd spike was used. Sm and Nd samples were loaded onto Re filaments of a double filament assembly. Sm and Nd isotopic analyses were carried out using a Finnigan MAT-262 mass spectrometer. Uncertainties on Sm/Nd and $^{143}Nd/^{144}Nd$ ratios are considered to be better than ±0.05% (1σ) and ±0.003% (1σ), respectively, based on repeated analyses of international rock standards BCR-1 and BHVO-1. The $^{143}Nd/^{144}Nd$ ratios were normalized to a $^{146}Nd/^{144}Nd$ ratio of 0.7219. Nd blanks were less than 100 pg.

The isotopic study was performed by calculating the ratios of Sm and Nd isotopes ($^{147}Sm/^{144}Nd$ and $^{143}Nd/^{144}Nd$), and εNd(0) notation from T_{DM} (Depleted Mantle) model ages (De Paolo, 1981, 1988).

Twenty-one samples of metaultramafic and metamafic rocks were analyzed. The isotopic data are shown in Table 4.

The rocks tend to present the original isotopic characteristics of the mantle-crust differentiation process. However, due to metamorphism and crustal reworking processes the isotopic composition may be disrupted (Burton and O'Nions, 1992; Tassinari et al., 2004; Barbosa et al., 2013). The isotopic system for the rock samples of this study is characterized by a rather restricted variation of Sm/Nd ratios (0.1102–1.1741), which may be related to combinations of Sm and/or Nd contents of each sample. The obtained Sm/Nd ratios are relatively low for mafic rocks, which is reflected in inconsistent (high Sm and Nd) contents compared to the original composition of the rocks (Lesnov, 2010; Rollinson, 1993).

According to De Paolo and Wasseburg (1976), the εNd(0) parameter is obtained by the difference between the $^{147}Sm/^{144}Nd$ ratio of the sample (or suite) and the CHUR reference value (Rollinson, 1993). The values obtained for the rocks of this study are extremely negative (Table 4).

The T_{DM} model ages for chloritites are between 2.06 and 2.25 Ga (Palaeoproterozoic), and for serpentinite the T_{DM} age is Mesoarchean (3.29 Ga). Table 4 shows that the εNd(0) values and TDM ages are similar to metamafic rocks of the Bonsucesso and Caraúbas formations. Most samples present Paleoproterozoic ages, with values between 1.99 and 2.46 Ga, as shown in the histogram of Fig. 11.

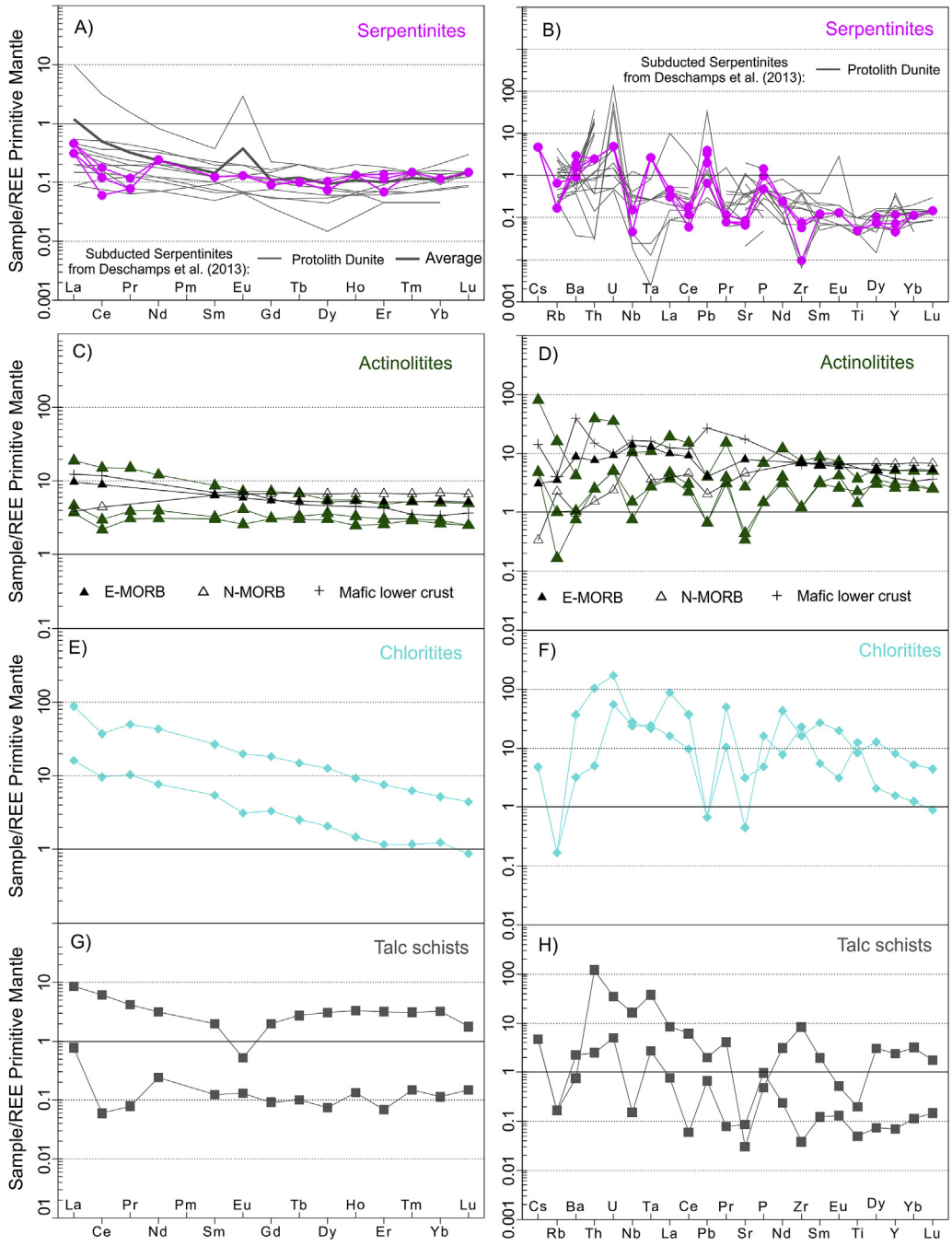

Fig. 6. REE distribution pattern and multi-element diagram normalized to the primitive mantle (McDonough and Sun, 1995) for the metaultramafic rocks compare with the subducted serpentinites from Deschamps et al. (2013); E- and N-MORB from Sun and McDonough (1989) and mafic lower crust from Rudnik and Gao (2003).

6. Discussion

6.1. Metaultramafic rocks

Minerals of the spinel group are highly resistant when undergoing hydrothermal alteration processes (e.g., serpentinization) or regional metamorphism (Burkhard, 1992). Depending on the alteration grade affecting the relict Cr-spinel crystals (Cr-magnetite and ferrichromite rims) the metamorphic grade condition can be inferred. A similar situation is observed in the Cr-spinel crystals that occur in some of the Morro dos Pereiras rocks, which indicates the variation in metamorphic grade from greenschist facies to amphibolites facies (Burkhard, 1992; Barnes, 2000; Ahmed et al., 2005; Azer and Khalil, 2006; Azer and Stern, 2007; Kapsiotis et al., 2007; Farahat, 2008; De Hoog et al., 2011; Samour and Hattori, 2013).

More than 900 chemical analyses of serpentinites were compiled by Deschamps et al. (2013). According to these authors, the geochemical standard of serpentinites is influenced by the tectonic setting were they are generated, the composition being a function of the formation temperature and the nature of the hydration fluids. From these parameters three types of serpentinites can be distinguished in subduction zones: i) abyssal serpentinites, formed by the hydration of peridotites due to hydrothermal

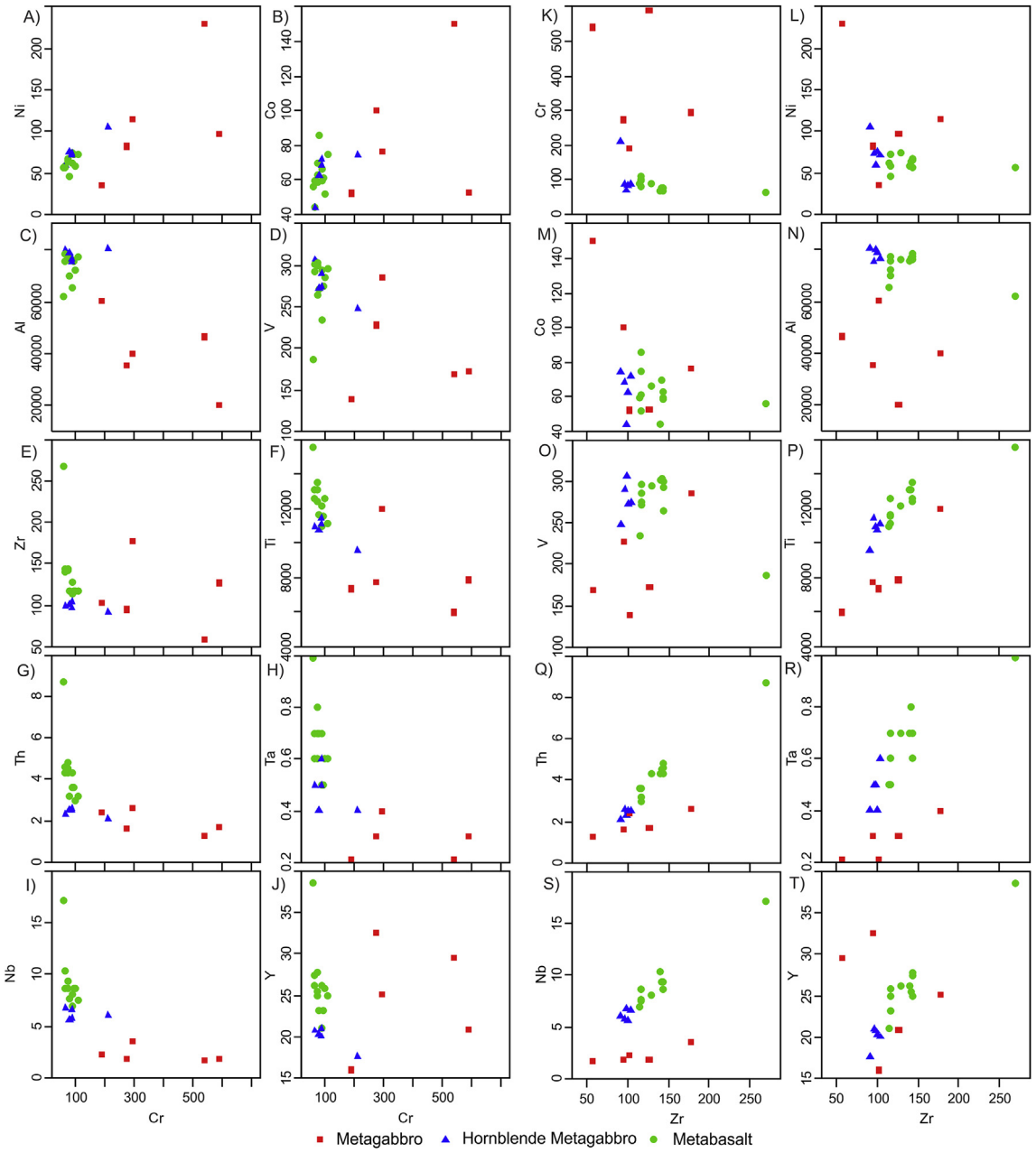

Fig. 7. Variation diagrams for the metamafic rocks: A) Ni x Cr; B) Co x Cr; C) Al x Cr; D) V x Cr; E) Zr x Cr; F) Ti x Cr; G) Th x Cr; H) Ta x Cr; I) Nb x Cr; J) Y x Cr.

activity; ii) mantle wedge serpentinites, formed by the interaction of fluids liberated by the subducted plates and later peridotite alteration, and iii) serpentinites formed in subduction zones, mainly found in suture zones and associated with high-pressure and low-temperature metamorphic rocks. They can be originated from abyssal peridotites hydrated in the subduction channel or from the Ocean-Continental Transitional Zone (OCT, Boillot et al., 1980; Manatschal et al., 2001; Whitmarsh et al., 2001).

The REE distribution in Morro dos Pereiras serpentinites is similar to the pattern presented by subduction zone serpentinites generated from exhumed sub-continental peridotites and hydrated during rifting of an ocean-continental transition zone (OCT), as proposed by Deschamps et al. (2013). The enrichment can be related to fluids rich in mobile elements coming from metasedimentary rocks (accretionary prism) before serpentinization in the subduction channel takes place (Deschamps, 2010; Lafay et al., 2013).

The actinolitites are characterized as the most differentiated ultramafic rocks in the study area, presenting Al and REE enrichment, with fractionation from LREE to HREE. These rocks may be ultramafic intrusions associated with serpentinized harzburgites and dunites. The chloritites present geochemical signature typical of mafic rocks, with high Al and Ti contents, enrichment in REE, and fractionation from LREE to HREE. The talc schists also present high Al contents and U-shaped pattern REE enrichment.

6.2. Metamafic rocks

The geochemical study of whole rock characterized the three rock groups in terms of degree of evolution, cogeneticity, and tectonic setting. The variation diagrams classified the metagabbros as the most primitive group, and the hornblende metagabbros and

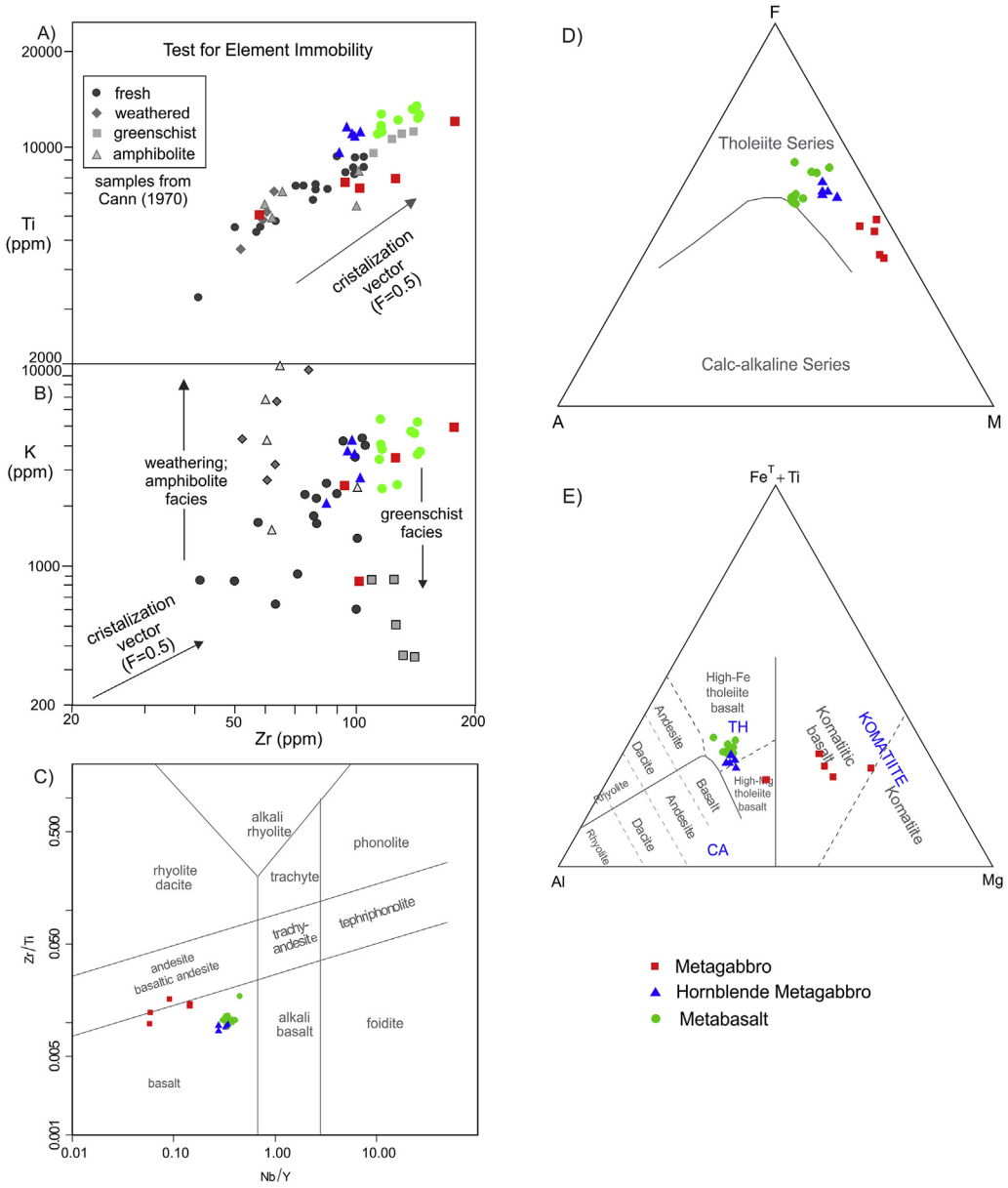

Fig. 8. Test for element immobility after Cann (1970) and Pearce (2014) – plots for metamafic rocks in the Zr x Ti (A) and (B) Zr x K diagrams; C) Plots in the Nb/Y x Zr/Ti diagram from Pearce (1996); D) Plots in the $Na_2O + K_2O$ x $Fe_2O_3^T$ x MgO (AFM) diagram from Irvine and Baragar (1971); E) Plots in the FeT + Ti x Al x Mg diagram from Jensen (1976).

metabasalts as the most evolved groups. In several diagrams, the metagabbros show different behavior from the other groups, indicating distinct genetic relationship regarding the sources.

The discriminant diagrams suggest an oceanic environment for mafic magma formation, associated with a strong crustal component. The signature ranges from basalts of ocean floor and mid-ocean ridge (MORB) to rocks formed in intra-plate environment, analogous to a continental rift in an OCT type of environment (Ocean Continental Transition). Contamination by crustal components may be observed in the displacement of samples towards Th in the triangular system of Wood (1980) – Fig. 10D, and in the Nb/Yb x Th/Yb diagram of Pearce 2008 – Fig. 12A.

The pattern marked by an oceanic signature with a strong crustal component is similar to the rocks formed from the interaction between mantle plumes and a strongly thinned continental crust, as in a passive margin in the ocean-continent transition (OCT) setting (Pearce, 2008; Caxito et al., 2014, Fig. 12B).

The context is coherent with the environment proposed by Ganade de Araújo et al. (2010), in which the protolith of metamafic rocks of the Novo Oriente Group would represent magmatism associated with a magma-poor passive margin (Whitmarsh et al., 2001; Franke, 2013) – Fig. 13. In this environment, the distribution of mafic rocks in the OCT is marked by a compositional variation, where the most enriched geochemical signatures (e.g. E- or P-MORB) occur near the continental margin while the N-MORB signatures are increasingly frequent toward the oceanic spreading center (Desmurs et al., 2002).

6.3. Tectonic implications and regional correlation

Precambrian ophiolites generated in transitional environments are scarce in the literature, mainly because of the complex

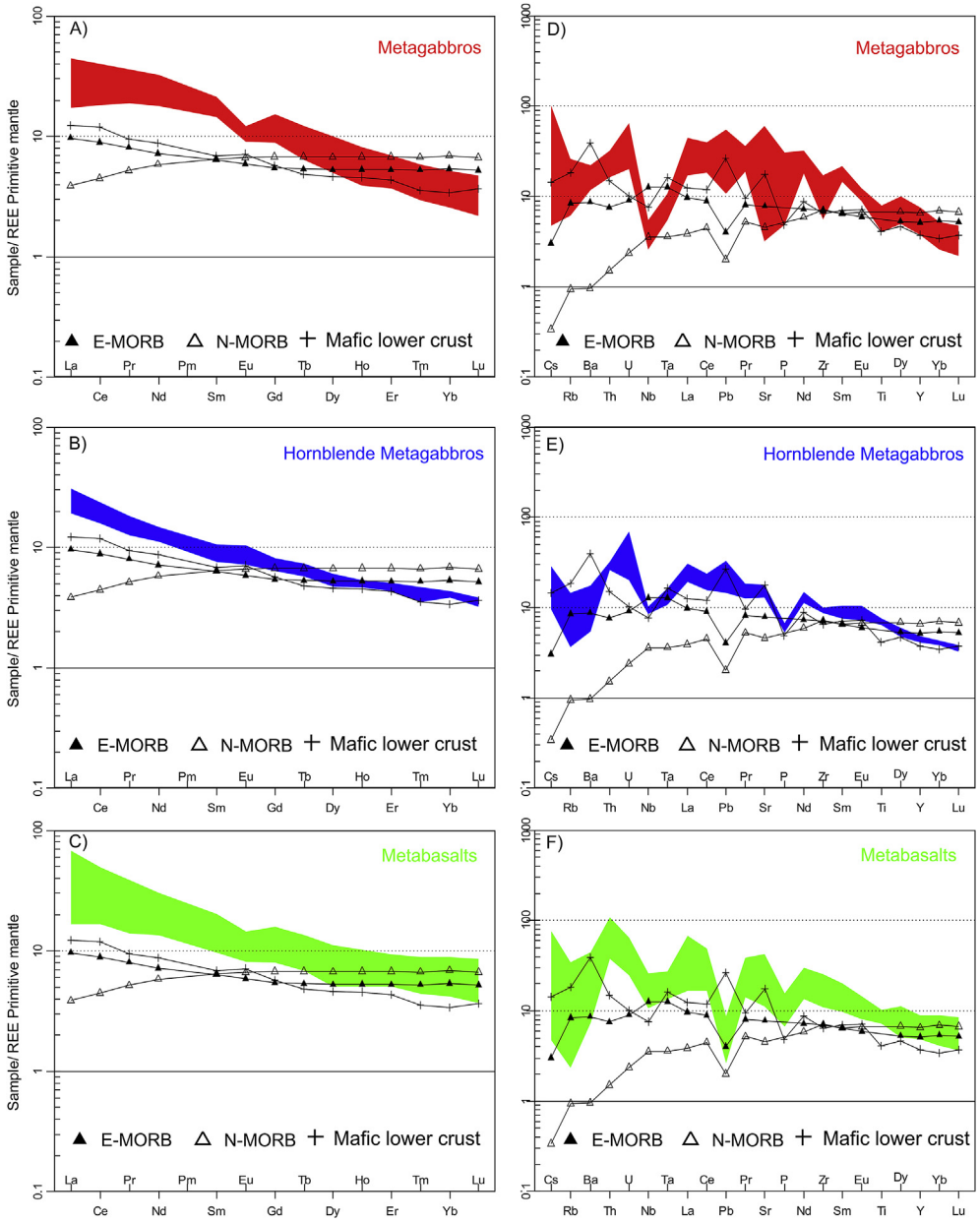

Fig. 9. REE distribution pattern and multi-element diagram normalized to the primitive mantle (McDonough and Sun, 1995) for the metamafic rocks, compare with the E- and N-MORB from Sun and McDonough (1989); mafic lower crust from Rudnik and Gao (2003).

evolutionary history of the planet that deletes these records. Examples of transitional ophiolites (Kusky, 2004) or continental margin type (CMT) ophiolites are described in the Paleoproterozoic Jormua Complex, in Finland (Kontinen, 1987; Peltonen et al., 2003), and also in some parts of the Slave Province, in Canada (Corcoran et al., 2004).

The mafic/ultramafic complex of Jormua (1.95 Ga) includes pillow lavas, volcanic breccias, complex mafic dykes, and peridotites of highly tectonized mantle. It occurs in the central part of a Paleoproterozoic metasedimentary sequence (2.3–1.92 Ga) in northeastern Finland (Peltonen et al., 2003). The geological context of the Novo Oriente region bears some lithological and geochemical similarities to the rocks of the Jormua Complex, reinforcing the possibility that the studied region may also have been formed in a passive margin environment in the ocean-continent transition.

It is uncertain when emplacement of the rift that would have given rise to magma-poor passive margin took place, due to lack of accurate absolute ages, and the Sm-Nd isochron ages couldn't be calculated for the Novo Oriente metabasalts. Thus, we may consider the following hypotheses for the opening of the inferred Novo Oriente rift:

(1) ca. 2.1 Ga: hypothesis supported by Sm-Nd isotopic data presented in this study, and by the U-Pb zircon age of approximately 2.1 Ga on a metabasalt of the Bonsucesso Formation (Ganade de Araújo et al., 2010).
(2) ca. 1.57 Ga: based on isotopic data, Ganade de Araújo et al. (2010) propose that the basin in focus may correspond to a more evolved stage of the ca. 1.57 Ga Mesoproterozoic extensional event recorded northwards, in the Forquilha region (Amaral et al., 2015);

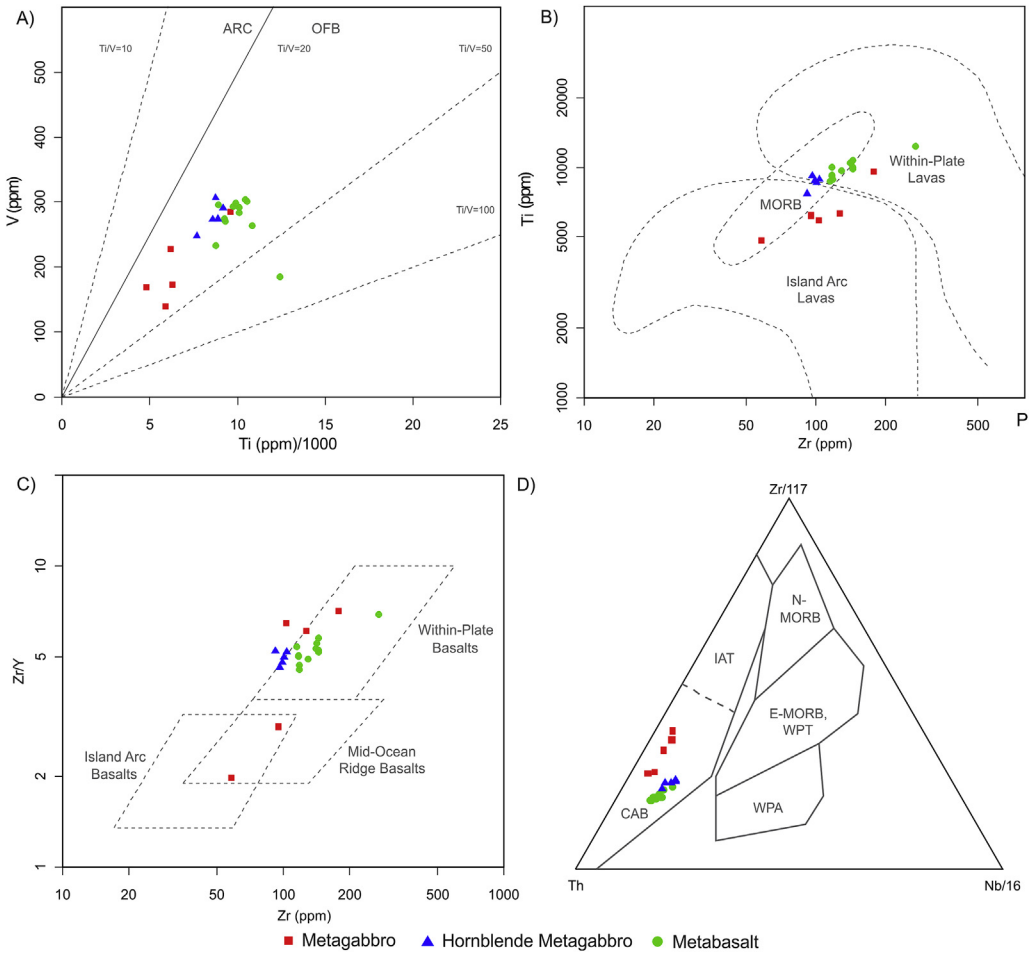

Fig. 10. Tectonomagmatic discrimination diagrams for the metamafic rocks: A) Ti x V (Shervais, 1982); B) Zr x Ti (Pearce, 1982); C) Zr x Zr/Y (Pearce and Norry, 1979); D) Triangular system Th-Hf-Ta-Zr-Nb of Wood (1980).

(3) ca. 0.95–0.8 Ga: also proposed by Ganade de Araújo et al. (2010) the age interval is related to the development of a passive margin resulting from the Rodinia Supercontinent breakup.

The U-Pb zircon age of 2083 ± 28 Ma obtained on metabasalt of Desterro, close to Quiterianópolis, is considered uncertain (Ganade de Araújo et al., 2010). However, if we assume the age value as the crystallization age of basalts, added to the Sm-Nd data presented here, the installation and development of the Novo Oriente rift would correlate with the generation of a magma-poor passive margin during the Paleoproterozoic (ca. 2.0–2.1 Ga).

Alternatively, the metamafic rocks of the Novo Oriente Group may be correlated to mafic rocks of high metamorphic grade of the Forquilha Eclogite Zone (Santos et al., 2009, 2015; Amaral 2010a; Amaral et al., 2010b, Amaral et al., 2015; Ancelmi et al., 2013, 2015), exposed approximately 240 km north of Novo Oriente. In this region, the authors identified three groups of metamafic rocks: i) garnet amphibolite with signature of island arc basalts (IAT); ii) retroeclogites with similar pattern to N-T MORB, compatible with basalts of mid-ocean ridge or back arc of intra-oceanic arcs; and iii) clinopyroxene-garnet amphibolite with alkaline basalt and continental basalt signature. From U-Pb, Sm-Nd and Lu-Hf geochronological data, the same authors proposed that some of these rocks were formed during an extensional event in the Mesoproterozoic, at about 1.5–1.6 Ga.

This period is compatible with Mesoproterozoic Nd T_{DM} ages of 1.36–1.69 Ga obtained in metamafic and metaultramafic rocks from Novo Oriente (Ferreira, 2008; Ganade de Araújo et al., 2010). However, analytical aspects such as the small number of Mesoproterozoic Nd T_{DM} ages indicate the need for further geochronological studies (e.g. U-Pb and Lu-Hf) in order to corroborate the earlier findings. Furthermore, the age of 1.36 Ga obtained by Ferreira (2008) suggests that the protolith of metamafics may have crystallized in a more recent event than the one recorded in Forquilha, dated at 1.57 Ga.

The period of continental rifting, development of passive margins, ocean spreading, subduction and continental collision related to the development of West Gondwana in the Borborema Province is still debatable. Despite the limited support from geological data, some authors argue the period around 800 Ma as the age of the initial rifting stage in the Borborema Province (Fetter et al., 2003; Castro, 2004; Arthaud, 2008).

Van Schmus et al. (2008) believe that the break-up of a Paleoproterozoic supercontinent during the Mesoproterozoic-Early Neoproterozoic created a vast region between the São Francisco-Congo and Amazon/West Africa cratons, consisting of extensional basins developed on the Archean-Paleoproterozoic crust and leading to small oceans – one of which could be represented by the Novo Oriente metamafic/metaultramafic rocks - and a large ocean along the main axis of the Transbrasiliano Kandi-shear system.

Caby (2014) studied the nature and evolution of a Neoproterozoic ocean-continent transition based on evidence in the

Table 4
Sm-Nd data of the metaultramafic and metamafic rocks of the Novo Oriente region. *Samples from Ganade de Araújo et al. (2010).

Sample	Rock	Sm (ppm)	Nd (ppm)	$^{147}Sm/^{144}Nd$	$^{143}Nd/^{144}Nd \pm 2\sigma$	ε_{Nd} (0)	T_{DM} (Ga)
NOJP-01A	MG	9.185	42.376	0.1310	0.5118 ± 06	−16.42	2.29
NOJP-01B	MG	8.141	39.210	0.1255	0.5118 ± 13	−16.85	2.18
NOJP-01C	MG	6.379	34.983	0.1102	0.5117 ± 29	−16.66	1.99
NOJP-01D	MG	8.273	41.694	0.1199	0.5118 ± 06	−17.19	2.08
NOJP-02	MG	6.998	35.552	0.1190	0.5117 ± 14	−17.68	2.11
NOJP-04A	CHL	6.084	30.639	0.1200	0.5118 ± 15	−16.92	2.06
NOJP-04B	CHL	2.208	9.967	0.1339	0.5119 ± 08	−15.23	2.25
NOJP-04C	SP	0.046	0.179	0.1564	0.5118 ± 70	−15.79	3.29
NOJP-08A	MB	5.356	23.124	0.1400	0.5119 ± 18	−14.74	2.39
NOJP-08B	MB	4.313	18.900	0.1379	0.5119 ± 15	−13.70	2.22
NOJP-08C	MB	4.688	16.976	0.1669	0.5121 ± 12	−11.32	3.29
NOJP-08D	MB	4.679	19.883	0.1422	0.5120 ± 12	−11.77	2.14
NOJP-08E	MB	5.284	22.129	0.1443	0.5120 ± 10	−13.22	2.37
NOJP-08F	MB	4.708	18.980	0.1499	0.5120 ± 12	−12.19	2.46
NOJP-08G	MB	4.606	19.518	0.1426	0.5121 ± 16	−11.39	2.11
NOJP-08H	MB	9.572	43.974	0.1316	0.5118 ± 04	−15.53	2.22
NOJP-08I	MB	4.743	18.771	0.1527	0.5120 ± 11	−12.61	2.63
NOJP-09A	HMG	3.790	16.255	0.1409	0.5120 ± 11	−12.13	2.14
NOJP-09B	HMG	4.695	21.113	0.1344	0.5118 ± 21	−15.83	2.33
NOJP-09C	HMG	3.437	14.452	0.1438	0.5120 ± 06	−11.55	2.16
NOJP-09D	HMG	4.394	18.687	0.1421	0.5120 ± 09	−12.06	2.17
*KE-417	MB	5.436	23.595	0.1393	0.511859 ± 09	−15.19	2.42
*KE-421B	HMG	3.814	15.607	0.1477	0.511975 ± 13	−12.92	2.46
*KE-278	Metaultramafic rock	3.276	16.136	0.1227	0.512026 ± 17	−11.93	1.69
*JC-36	Metamafic rock	4.069	20.573	0.1199	0.512080	−10.53	1.53

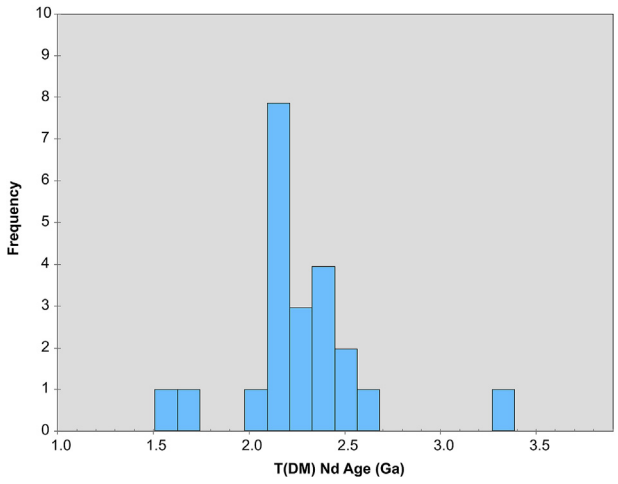

Fig. 11. Histogram showing the distribution of TDM Nd ages for the metaultramafic and metamafic rocks of the Novo Oriente region.

Timétrine massif, on the margin of the West African craton, NE Mali. According to the author, it is possible to reconstruct the former ocean-continent transition similarly to that evidenced for the Mesozoic Era, followed by the deposition of syn-to post rift terrigeneous turbidites, roughly coeval with ocean spreading some time before 800 Ma. Caby (2014) concluded that first the serpentinite massifs were tectonically emplaced in an extensional setting, then incorporated within deep-sea sediments as olistoliths, and finally transported westward during late Neoproterozoic collisional tectonics onto the West African craton.

In this context, the early stages of the Novo Oriente rift may be related to this extensional Meso-Neoproterozoic event, forming part of the passive margin system developed during Rodinia breakup (ca. 0.95–0.8 Ga) associated with a pre-Brasiliano/Pan African ocean (e.g. Goiás-Pharusian Ocean, Ganade de Araújo et al., 2010).

7. Conclusions

From field data, plus petrographic, geochemical and Nd isotope studies, we conclude that:

- The Morro dos Pereiras area is composed of a sequence of metaultramafic rocks intercalated with a metasedimentary sequence. The metaultramafic sequence comprises dominant deformed and undeformed serpentinites, chloritites, actinolitites, talc-chlorite schists, serpentine-talc schists, talc-rich siliceous rocks and subordinated listwänites.
- The geochemical data indicate that the serpentinites correspond to rocks originated by the alteration of dunites depleted in HREE, similar to the pattern presented by subduction-zone serpentinites generated from exhumed sub-continental peridotites and hydrated during ocean-continent transition (OCT) rifting. The protoliths may have formed from depleted products resulting from the upper mantle partial melting. As a result of this process, the ultramafic restites are considerably depleted in REE, in contrast with the REE-enriched serpentinites, actinolitites, talc schists and chloritites are.
- The lithogeochemical data indicate that protoliths of metamafic rocks consist of basic rocks of basaltic composition and tholeiitic affinity. The most primitive term is represented by metagabbros, and the most evolved by metabasalts. They present signatures between E- and N-MORB with variable contamination by crustal components, similar to the rocks formed from the interaction between mantle plumes and a strongly thinned continental crust, as in a passive margin in the ocean-continent transition (OCT).
- The isotopic analyses indicate strong crustal assimilation for the studied rocks, as evidenced by strongly negative εNd with values ranging from −11.32 to −17.68 and essentially Paleoproterozoic T_{DM} ages (2.06 and 2.25 Ga). T_{DM} ages are compatible with the U-Pb age of about 2.1 Ga of metabasalt from the Bonsucesso Formation.
- Based on isotopic data available for metamafic rocks of the Novo Oriente Group and regional correlations, three scenarios are possible for formation of the rift that originated the basin: i)

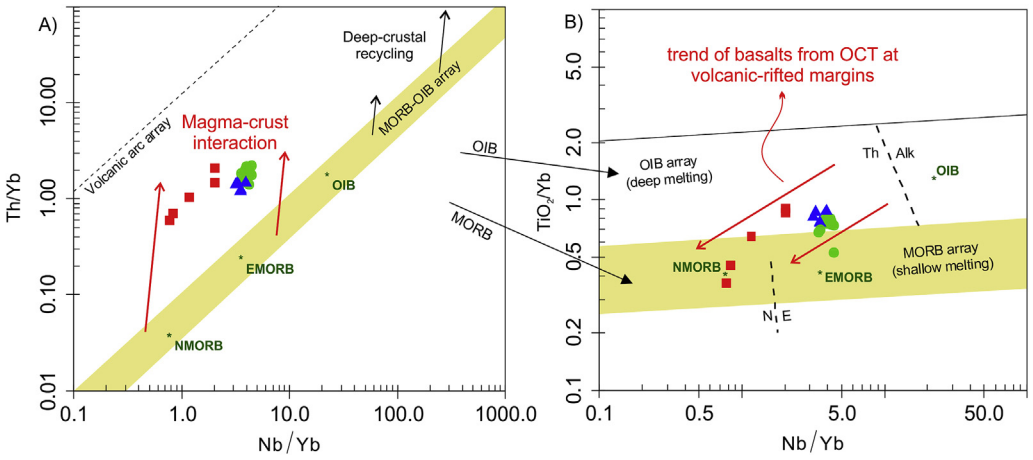

Fig. 12. Plots in the Nb/Yb x Th/Yb (A) and Nb/Yb x TiO2/Yb (B) of Pearce (2008) for the Novo Oriente metamafic rocks.

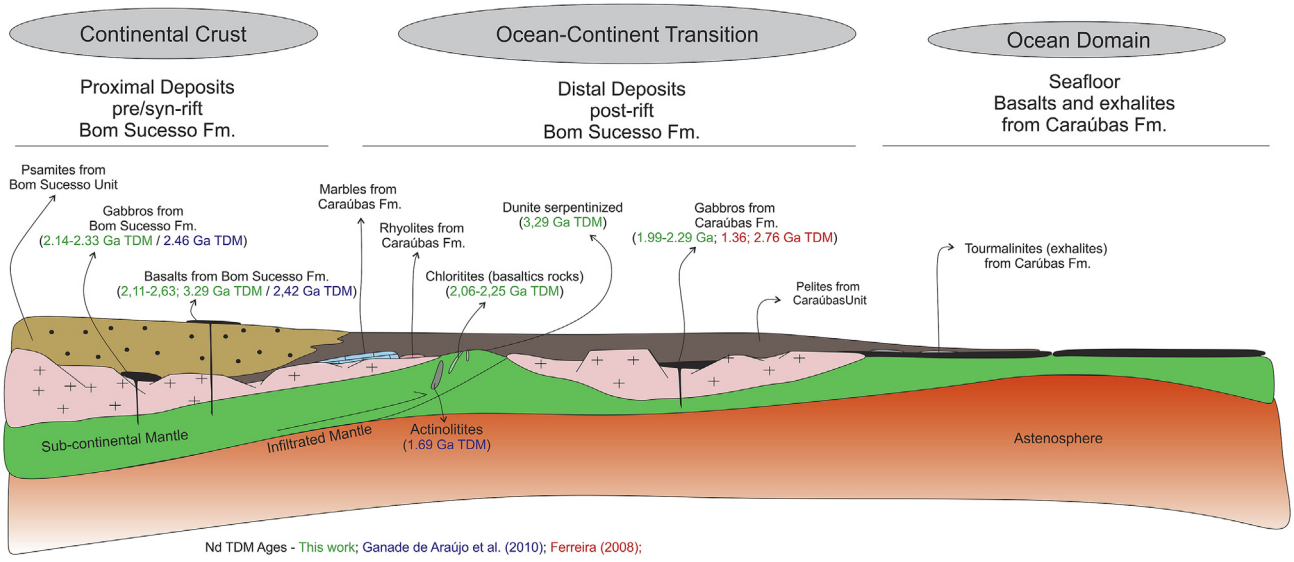

Fig. 13. Geotectonic scenario for the Novo Oriente ocean-continental transition and distribution of the Sm-Nd isotopic data of the metaultramafic and metamafic rocks.

related to the generation of a magma-poor passive margin in the Paleoproterozoic (ca. 2.0–2.1 Ga); ii) as a more evolved stage of an extensional Mesoproterozoic event recorded in Forquilha at *ca.* 1.57 Ga; and iii) associated with the development of a passive margin resulting from the Supercontinent Rodinia breakup (ca. 0.95–0.8 Ga).

Acknowledgements

This paper is part of research carried out in cooperation between the Department of Geology of the Federal University of Ceará and the Geosciences Institute of UNB. The authors wish to thank the CAPES (Coordenação de Aperfeiçoamento de Pessoal de Nível Superior) for funding of academic cooperation project entitled: 'Contexto Geológico/Geotectônico dos Recursos Minerais do Estado do Ceará". PROCAD-NF. The authors wish to thank the Instituto Nacional de Ciência e Tecnologia de Estudos Tectônicos (CNPq/INCT-ET/grant 573713/2008-1 to RAF), for the financial support. To University of Ceará (UFC), and University of Campinas (UNICAMP) for technical and laboratorial support. JPAP are grateful to CAPES (Coordenação de Aperfeiçoamento de Pessoal de Nível Superior) for research scholarships. WSA, RAF and ELT are also grateful to CNPq – *Conselho Nacional de Desenvolvimento Científico e Tecnológico,* for research scholarships.

References

Ahmed, A.H., Arai, S., Abdel-Azis, Y.M., Rahimi, A., 2005. Spinel composition as a petrogenetic indicator of the mantle section in the Neoproterozoic Bou Azzer ophiolite, Anti-Atlas, Morocco. Precambrian Res. 138, 225–234.

Almeida, F.F.M., Hasui, Y., Brito Neves, B.B., Fuck, R.A., 1981. Brazilian structural provinces. Earth Sci. 7, 1–29.

Amaral, W., Santos, T.J., Ancelmi, M.F., Fuck, R.A., Dantas, E.L., Matteini, M., Moreto, C.P., 2015. 1.57 Ga protolith age of the Neoproterozoic Forquilha eclogites, Borborema Province, NE-Brazil, constrained by U–Pb, Hf and Nd isotopes. J. S. Am. Earth Sci. 58, 210–222.

Amaral, W.S., Santos, T.J.S., Wernick, E., 2010b. Occurrence and geochemistry of metamafic rocks from the Forquilha eclogite zone, central Ceará (NE Brazil): geodynamic implications. Geol. J. 46 (2–3), 137–155.

Amaral, W.S., Santos, T.J.S., Wernick, E., 2011. Occurrence and geochemistry of metamafic rocks from the Forquilha Eclogite Zone, central Ceará (NE Brazil): geodynamic implications. Geol. J. (Chichester) 46, 137–155.

Amaral, W.S., Santos, T.J.S., Wernick, E., Nogueira Neto, J.A., Dantas, E.L., Matteini, M., 2012. High-pressure granulites from Cariré, Borborema Province, NE Brazil: tectonic setting, metamorphic conditions and U Pb, Lu Hf and Sm Nd geochronology. Gondwana Res. 22, 892–909.

Amaral, W.S., 2010a. PhD. Thesis. Análise geoquímica, geocronológica e

termobarométrica das rochas de alto grau metamórfico, adjacentes ao arco magmático de Santa Quitéria, vol. 274. Universidade Estadual de Campinas-SP, NW da Província Borborema.
Ancelmi, M.F., Santos, T.J.S., Reginato, R.A., Amaral, W.S., Monteiro, L.V.S., 2013. Geologia da Faixa Eclogítica de Forquilha, Domínio Ceará Central, noroeste da Província Borborema. Brazilian J. Geol. 43, 235–252. http://dx.doi.org/10.5327/Z2317-48892013000200004.
Ancelmi, M.F., Santos, T.J.S., dos Amaral, W.S., Fuck, R.A., Dantas, E.L., Zincon, S.A., 2015. Provenance of metasedimentary rocks from the Ceará central domain of Borborema Province, NE Brazil: implications for the significance of associated retrograded eclogites. J. S. Am. Earth Sci. 58, 82–99.
Arthaud, M.H., 2008. Evolução Neoproterozóica do Grupo Ceará (Domínio Ceará Central, NE Brasil), da sedimentação à colisão continetal brasiliana. PhD. Thesis. Instituto de Geociências, Universidade de Brasília, Brasília, p. 170.
Azer, M., Stern, R.J., 2007. Neoproterozoic serpentinites in the eastern Desert, Egypt: fragments of fore-arc mantle. Geology 115, 457–472.
Azer, M.K., Khalil, A.E.S., 2005. Petrological and mineralogical studies of Pan-African serpentinites at Bir Al-Edeid area, central eastern Desert, Egypt. J. Afr. Earth Sci. 43, 525–536.
Azer, M.K., Khalil, A.E.S., 2006. Petrological and mineralogical studies of Pan-African serpentinites at Bir Al-Edeid area, central eastern Desert, Egypt. J. Afr. Earth Sci. 43, 525–536.
Barbosa, N.S., Teixeira, W., Leal, L.R.B., Leal, A.B.M., 2013. Evolução crustal do setor ocidental do Bloco Arqueano Gavião, Cráton do São Francisco, com base em evidências U-Pb, Sm-Nd e Rb-Sr. Geol. USP. Sér. Cient., São Paulo 13 (4), 6–88.
Barnes, S.D., 2000. Chromite in Komatiites, II. Modification during greenschist to mid amphibolite facies metamorphism. J. Petrol. 41, 387–409.
Bodinier, J.L., Dupuy, C., Dostal, J., 1984. Geochemistry of precambrian ophiolites from Bou Azzer, Morocco. Contrib. Mineral. Petrol. 87, 43–50.
Boillot, G., Froitzheim, N., 2001. Non-volcanic rifted margins, continental break-up and the onset of sea-floor spreading: some outstanding questions. In: Wilson, R.C.L., et al. (Eds.), Non-volcanic Rifting of the Continental Margins: a Comparison of Evidence from Land and Sea, vol. 187. Geological Society Special Publication, pp. 9–30.
Boillot, G., Grimaud, S., Mauffret, A., Mougenot, D., Kornprobst, J., Mergoil-Daniel, J., Torrent, G., 1980. Ocean-continent boundary off the Iberian margin: a serpentinite diapir west of the Galicia Bank. Earth Planet. Sci. Lett. 48, 23–34.
Bousquet, R., Mamoun, R., Saddiqui, O., Goffé, B., Möller, A., Madi, A., 2008. Mélanges and ophiolites during the Pan-African orogeny: the case of the Bou Azzer ophiolite suite (Morocco). In: Ennih, N., Liégeois, J.P. (Eds.), The Boundary of the West African Craton, Geological Society London, vol. 297. Special Publications, pp. 233–247.
Brito Neves, B.B., Cordani, U.G., 1991. Tectonic evolution of south America during the late proterozoic. In: Stern, R.J., Van Schmus, W.R. (Eds.), Crustal Evolution in the Late Proterozoic: Precambrian Research, vol. 53, pp. 23–40.
Burkhard, D.I.M., 1992. Accessory chromium spinels: their coexistence and alteration in serpentinites. Geochim. Cosmochim. Acta 57, 1297–1306.
Burton, K.W., O'nions, R.K., 1992. The timing of mineral growth across regional metamorphic sequence. Nature 357, 235–238.
Caby, R., 1989. Precambrian terranes of Benin Nigeria and northeast Brazil and late proterozoic south Atlantic fit. Geol. Soc. Am. Special Pap. 230, 145–158.
Caby, R., 2014. Nature and evolution of Neoproterozoic ocean-continent transition: evidence from the passive margin of the West African craton in NE Mali. J. Afr. Earth Sci. 91, 1–11.
Cann, J.R., 1970. Rb, Sr, Y, Zr and Nb in some ocean fl oor basaltic rocks. Earth Planet. Sci. Lett. 10, 7–11.
Castro, N.A., 2004. Evolução geológica proterozóica da região entre Madalena e Taperuaba, domínio tectônico Ceará Central (Província Borborema). Phd thesis. Universidade de São Paulo, Brazil, p. 212.
Castro, N.A., Ganade de Araujo, C.E., Basei, M.A.S., Osako, L.S., Nutman, A.A., Liu, D., 2012. Ordovician a-type granitoid magmatism on the Ceará central domain, Borborema Province, NE-Brazil. J. S. Am. Earth Sci. 36, 18–31.
Cavalcante, J.C., Vasconcelos, A.M., Medeiros, M.F., Paiva, I.P., Gomes, F.E.M., Cavalcante, S.N., Cavalcante, J.E., Melo, A.C.R., Duarte Neto, V.C., Benevides, H.C., 2003. Mapa Geológico do Estado do Ceará – Escala 1:500.000.Fortaleza. Ministério das Minas e Energia, CPRM.
Caxito, F.A., Uhlein, A., Stevenson, R., Uhlein, G.J., 2014. Neoproterozoic oceanic crust remnants in northeast Brazil. Geol. (Boulder, Colo.) 42, 387–390.
Corcoran, P.L., Mueller, W.U., Kusky, T.M., 2004. Inferred Ophiolites in the Archean Slave Craton. In: Kusky, T.M. (Ed.), Precambrian Ophiolites and Related Rocks, Developments in Precambrian Geology, 13. Elsevier, Amsterdan, pp. 363–404.
Costa, F.C., Araújo, C.E.G., Amaral, W.S., Vasconcelos, A.M., Rodrigues, J.B., 2013. U-Pb (LA-ICPMS) Zircon Ages and Nd Isotopes for Granitoids of the Tamboril-Santa Quitéria Complex, Ceará Central Domain: Implication for Neoproterozoic Syn-collisional Magmatism in North Borborema Province, vol. 13. Geologia USP - Série Científica, pp. 159–174.
De Hoog, J.C.M., Janák, M., Vrabec, M., Hattori, K.H., 2011. Ultramafic cumulates of oceanic affinity in an intracontinental subduction zone: ultrahigh-pressure garnet peridotites from Pohorje (Eastern Alps, Slovenia). In: Dobrzhinetskaya, L., Cuthbert, S., Faryad, W. (Eds.), Ultrahigh Pressure Metamorphism. Elsevier, Amsterdam.
De Paolo, D.J., 1981. Neodimium isotopes in the Colorado front range and crust-mantle evolution in the proterozoic. Nature 291, 193–196.
De Paolo, D.J., 1988. Neodymium Isotope Geochemistry. Springer-Verlag, Berlin, p. 187.
De Paolo, D.J., Wasseburg, G.J., 1976. Inferences about magma sources and mantle structure from variations 143Nd/144Nd. Geophys. Res. Lett. 3, 743–746.
Deschamps, F., 2010. Caractérisation in situ des serpentines en contexte de subduction: de la nature àl'expérience. Phd Thesis. Université Joseph Fourier, Grenoble, p. 402.
Deschamps, F., Godard, M., Guillot, S., Hattori, K., 2013. Geochemistry of subduction zone serpentinites: a review. Lithos 178, 96–127.
Desmurs, L., Müntener, O., Manatschal, G., 2002. Onset of magmatic accretion within a magma-poor rifted margin: a case study from the platta ocean-continent transition, eastern Switzerland. Contrib. Mineral. Petrol. 144, 365–382.
Dilek, Y., Furnes, H., 2011. Ophiolite genesis and global tectonics: geochemical and tectonic fingerprinting of ancient oceanic lithosphere. Bull. Geol. Soc. Am. 123, 387–411.
Dilek, Y., Furnes, H., 2014. Ophiolites and their origins. Elements 10, 93–100.
Dilek, Y., Robinson, P.T., 2003. Ophiolites in Earth history: introduction. In: Dilek, Y., Robinson, P.T. (Eds.), Ophiolites in Earth History. Geological Society of London, vol. 218. Special Publications, pp. 1–8.
El Hadj, T.M., Affaton, P., Louis, P., Socohou, A., 1997. Gravity characteristics of the Pan-African orogen in Ghana, Togo and Benin (West Africa). J. Afr. Earth Sci. 7, 241–258.
Farahat, E.S., 2008. Chrome-spinels in serpentinites and talc carbonates of the El Ideid-El Sodmein District, central Eastern Desert, Egypt: their metamorphism and petrogenetic implications. Chem. Erde Geochem. 68, 196–205.
Ferreira, I.G., 2008. Aspectos geológicos, estruturais e geocronológicos da Seqüência Metavulcano-Sedimentar de Novo Oriente-CE. Masters Dissertation. Universidade Federal do Ceará.
Fetter, A.H., 1999. U-Pb and Sm-Nd geochronological constraints on the crustal framework and geologic history of Ceará State, NW Borborema Province, NE Brazil: implications for the assembly of Gondwana. PhD. Thesis. Dept. of Geology, Kansas University, USA, p. 164.
Fetter, A.H., Van Schmus, W.R., Santos, T.J.S., Arthaud, M., Nogueira Neto, J.A., 2000. U-Pb and Sm-Nd geochronological constrains on the crustal evolution and basement architecture of Ceará State, NW Borborema Province, NE Brazil: implications for the existence of the paleoproterozoic supercontinent Atlantica. Rev. Bras. Geociênc. 30, 102–106.
Fetter, A.H., Santos, T.J.S., Van Schmus, W.R., Hackspacher, P.C., Brito Neves, B.B., Arthaud, M.H., Nogueira Neto, J.A., Wernick, E., 2003. Evidence for neoproterozoic continental collisional granitoids in north Borborema Province arc magmatism in the Santa Quitéria Batholith of Ceará state, NW Borborema Province, NE Brazil: implications for the assembly of West Gondwana. Gondwana Res. 6, 265–273.
Franke, D., 2013. Rifting, lithosphere breakup and volcanism: comparison of magma-poor and volcanic rifted margins. Mar. Petroleum Geol. 43, 63–87.
Furnes, H., Dilek, Y., de Wit, M., 2013. Precambrian greenstone sequences represent different ophiolite types. Gondwana Res. 27 (2), 649–685.
Furnes, H., Dilek, Y., de Wit, M., 2015. Precambrian greenstone sequences represent different ophiolite types. Gondwana Res. 27, 649–685.
Ganade de Araújo, C.E., Pinéo, T.R.G., 2015. Geologia e recursos minerais da folha Novo Oriente - SB.24-V-C-VI. CPRM-SGB – Serviço Geológico do Brasil, Fortaleza-CE.
Ganade de Araújo, C.E., Pineo, T.R.G., Caby, R., Costa, F.G., Cavalcante, J.C., Vasconcelos, A.M., Rodrigues, J.B., 2010. Provenance of the Novo Oriente Group, southwestern Ceará Central Domain, Borborema Province (NE-Brazil): a dismembered segment of a magma-poor passive margin or a restricted rift-related basin? Gondwana Res. 6, 265–273.
Ganade de Araujo, C.E., Costa, F.G., Pinéo, T.R.G., Cavalcante, J.C., Moura, C.A.V., 2012. Geochemistry and 207Pb/206Pb zircon ages of granitoids from the southern portion of the Tamboril-Santa Quitéria granitic-migmatitic complex, Ceará central domain, Borborema Province (NE Brazil). J. S. Am. Earth Sci. 33, 21–33.
Ganade de Araújo, C.E.G., Pineo, T.R.G., Calado, B.O., Gomes, I., Cavalcante, J.C., 2011. Mapa Geológico da Folha Novo Oriente (SB-24-V-C-VI), CPRM-SGB – Serviço Geológico do Brasil, Fortaleza-CE, (escala 1:100.000).
Gioia, S.M.C.I., Pimentel, M.M., 2000. The Sm-Nd isotopic method in the geochronology laboratory of the University of Brasília. An. Acad. Bras. Ciências 72, 219–245.
Irvine, T.N., Baragar, W.R.A., 1971. A guide to the chemical classification of the common volcanic rocks. Can. J. Earth Sci. 8, 523–548.
Jensen, L.S., 1976. A New Cation Plot for Classifying Subalkaline Volcanic Rocks. Ontario Division of Mines, Misc., Paper 66.
Johnson, P.R., Kattan, F.H., Al-Saleh, A.M., 2004. Neoproterozoic ophiolites in the Arabian shield: field relations and structure. In: Kusky, T.M. (Ed.), Precambrian Ophiolites and Related Rocks, 120–162, Developments in Precambrian Geology 13 (K.C. Condie, Series Editor). Elsevier.
Kapsiotis, A., Grammatikopoulos, T., Karipi, S.T., Hatzipanagiotou, K., 2007. On the metamorphic modification of cr-spinel compositions from the ultrabasic rocks of the pindos ophiolite complex (nw Greece). Bull. Geol. Soc. Greece 781–793.
Kontinen, A., 1987. An early Proterozoic ophiolite—the Jormua mafic-ultramafic complex, northeastern Finland. Precambrian Res. 35, 313–341.
Kusky, T.M., 2004. Precambrian Ophiolites and Related Rocks. Developments in Precambrian Geology, 13. Elsevier, Amsterdan.
Lafay, R., Deschamps, F., Schwartz, S., Guillot, S., Godard, M., Debret, B., Nicollet, C., 2013. High-pressure serpentinites, a trap-and-release system controlled by metamorphic conditions: example from the Piedmont zone of the western Alps. Chem. Geol. 343, 38–54.

Le Bas, M.J., Streckeisen, A.L., 1991. The IUGS systematics of igneous rocks. J. Geol. Soc. Lond. 148, 825–833.
Lesnov, F.P., 2010. Rare earth elements in ultramafic and mafic rocks and their minerals, Library of Congress Cataloging-in-Publication Data, 1, 1–69.
Manatschal, G., Froitzheim, N., Rubenach, M.J., Turrin, B., 2001. Therole of detachment faulting in the formation of an ocean-continenttransition: insights from the Iberia Abyssal Plain. In: Wilson, R.C.L., Whitmarsh, R.B., Taylor, B., Froitzheim, N. (Eds.), Non-volcanic Rifting of Continental Margins: Evidence from Land and Sea. Geol Soc (London), vol. 187. Spec Publ., pp. 405–428
Manatschal, G., 2004. New models for evolution of magma-poor rifted margin based on a review of data and concepts from West Iberia and the Alps. Int. J. Earth Sci. 93, 432–466.
Manatschal, G, Müntener, O., 2009. A type sequence across an ancient magma-poor ocean–continent transition: the example of the western Alpine Tethys ophiolites. Tectonophysics 473, 4–19.
Martins, G., Oliveira, E.P., Lafon, J.M., 2009. The Algodões amphibolite-tonalite gneiss sequence, Borborema Province, NE Brazil: geochemical and geochronological evidence for Paleoproterozoic accretion of oceanic plateu/back-arc basalts and adakitic plutons. Gondwana Res. 15, 71–85.
McDonough, W.F., Sun, S.S., 1995. Composition of the earth. Chem. Geol. 120, 223–253.
Moores, E.M., 2002. Pre-1 Ga (Pré-Rodínia) ophiolites: their tectonic and environmental implications. GSA Bull. 114, 80–95.
Paixão, M.A.P., Nilson, A.A., Dantas, E.L., 2008. The Neoproterozoic Quatipuru ophiolite and the Araguaia fold belt, central-northern Brazil, compared with correlatives in NW Africa. In: Pamkhurst, R.J., Trouw, R.A.J., Brito-Neves, B.B., de, Wit M.J. (Eds.), West Gondwana: Pre-cenozoic Correlations across the South Atlantic Region, vol. 294. Geological Society of London, Special Publications, pp. 297–318.
Paixão, M.A.P., 2009. Complexo ofiolítico Quatipuru, pará, Brasil. Phd Thesis. Brasília: Instituto de Geociências, Universidade de Brasília, Brasília, p. 118.
Pearce, J.A., 1982. Trace element characteristicsof lavas from destructive plate boundaries. In: Thorpe, R.S. (Ed.), Andesites. Wiley, Chichester, pp. 525–548.
Pearce, J.A., 1996. A User's Guide to Basalt Discrimination Diagrams, vol. 12. Geological Association of Canada Special Publication, pp. 79–113.
Pearce, J.A., 2008. Geochemical fingerprinting of oceanic basalts with applications to ophiolite classification and the search for Archean oceanic crust. Lithos 100, 14–48.
Pearce, J.A., 2014. Immobile element fingerprinting of ophiolites. Elements 10, 101–108.
Pearce, J.A., Norry, M.J., 1979. Petrogenetic implications of Ti, Zr, Y, and Nb variations in volcanic rocks. Contrib. Mineral. Petrol. 69, 33–47.
Pedrosa-Soares, A.C., Vidal, P., Leonardos, O.H., De Brito Neves, B.B., 1998. Neoproterozoic oceanic remnants in eastern Brazil: further evidence and refutation of an exclusively ensialic evolution for the Araçuaí–West Congo orogen. Geology 26, 519–522.
Peltonen, P., Mänttäri, I., Huhma, H., Kontinen, A., 2003. Archean zircons from the mantle: the Jormua ophiolite revisited. Geology 31, 645–648.
Queiroga, G.N., Pedrosa-Soares, A.C., Noce, C.M., Alkmim, F.F., Pimentel, M.M., Dantas, E., Martins, M., Castañeda, C., Suita, M.T.F., Prichard, H., 2007. Age of the Ribeirão da Folha ophiolite, Araçuaí Orogen: the U-Pb zircon (LA-ICPMS) dating of a plagiogranite. Geonomos 15, 61–65.
Queiroga, G.N., Suita, M.T.F., Soares, A.C.P., Martins, M.S., Pinheiro, M.A.P., 2012. Síntese sobre ofiolitos: evolução dos conceitos. Geociênc. 65, 47–58.
Reston, T., Manatschal, G., 2011. Rifted Margins: Building Blocks of After Collision. Arc– Continent Collision. Frontiers in Earth Sciences Springer, Berlin Heidelberg, pp. 3–21.
Reston, T.J., 1993. Evidence for extensional shear zones in the mantle offshore Britain, and their implications for the extension of the continental lithosphere. Tectonics 12, 492–506.
Reston, T.J., 2009. The structure, evolution and symmetry of the magma-poor rifted margins of the North and Central Atlantic: a synthesis. Tectonophysics 468, 6–27.
Richard, P., Shimizu, N., Allegre, C.J., 1976. $^{143}Nd/^{144}Nd$, a natural tracer: an application to oceanic basalts. Earth Planet. Sci. Lett. 31, 269–278.
Rudnick R.L., Gao S., 2003. The Composition of the Continental Crust, pp. 1–64. In: The Crust (ed. R.L. Rudnick) Vol. 3, Treatise on Geochemistry (eds. H.D. Holland and K.K. Turekian), Elsevier-Pergamon, Oxford. 39-51.
Salem, A.K.A., Khalil, A.E., Ramadan, T.M., 2012. Geology, geochemistry and tectonic setting of Pan-African serpentinites of Um Salim-Um Salatit area, central eastern Desert, Egypt. Egypt. J. Remote Sens. Space Sci. 15, 171–184.
Santos, T.J.S., Amaral, W.D.S., Ancelmi, M.F., Pitarello, M.Z., Fuck, R.A., Dantas, E.L., 2015. U–Pb age of the coesite-bearing eclogite from NW Borborema Province, NE Brazil: implications for western Gondwana assembly. Gondwana Res. 28, 1183–1196.
Santos, T.J.S., Garcia, M.G.M., Amaral, W.S., Caby, R., Wernick, E., Arthaud, M.H., Dantas, E.L., Santosh, M., 2009. Relics of eclogite facies assemblages in the Ceará central domain, NW Borborema Province, NE Brazil: implications for the assembly of West Gondwana. Gondwana Res. 15, 454–470.
Saumur, B.-M., Hattori, K.H., 2013. Zoned Cr-spinel in forearc serpentinites along the northern Caribbean Margin, Dominican Republic. Mineral. Mag. 77, 117–136.
Shervais, J.W., 1982. Ti-V plots and the petrogenesis of modern and ophiolitic lavas. Earth Planet. Sci. Lett. 59, 101–118.
Stern, R.J., Johnson, P.R., Kröner, A., Yibas, B., 2004. Neoproterozoic ophiolites of the Arabian-Nubian shield. In: Kusky, T.M. (Ed.), Precambrian Ophiolites and Related Rocks, 95–128. Developments in Precambrian Geology 13 (K.C. Condie, Series Editor). Elsevier.
Suita, M.T.F., Pedrosa-Soares, A.C., Leite, C., Nilson, A.A., Prichard, H., 2004. Complexos ofiolíticos do Brasil e a metalogenia comparada das faixas Araçuaí e Brasília. Complejos Ofiolíticos en Iberoamérica: guías de prospección para metales preciosos. Ciencia y Tecnología para el Desarrollo-CYTED, Madrid, pp. 101–132.
Sun, S.S., McDonough, W.F., 1989. Chemical and Isotopic Systematics of Oceanic Basalts; Implications for Mantle Composition and Processes, vol. 42. Geological Society of London Special Publication, pp. 313–345.
Tack, L., Wingate, M.T.D., Liégeos, J.P., Fernandes Alonso, M., Deblond, A., 2001. Early neoproterozoic magmatism (1000–900 Ma) of the Zadinian and Mayumbian groups (Bas Congo): onset of the Rodinia rifting at the West edge of Congo craton. Precambrian Res. 110, 277–306.
Tassinari, C.C., Munhá, J.M., Ribeiro, A., Correia, C.T., 2001. Neoproterozoic oceans in the Ribeira belt (southeastern Brazil): the pirapora do Bom Jesus ophiolitic complex. Episodes 24, 245–251.
Tassinari, C.C.G., Munhá, J.M.U., Teixeira, W., Palácios, T., Nutman, A.P., Cesar Sosa, S., Santos, A.P., Calado, B.O., 2004. The Imataca Complex, NW Amazonian Craton, Venezuela: crustal evolution and integration of geochronological and petrological cooling histories. Episodes 27 (1).
Trompette, R., 1994. Geology of Western Gondwana, Pan-African (2000-500 Ma)–Pan-african Brasiliano Aggregation of South America and Africa. A. A. Balkema, Rotterdam, p. 350.
Van Schmus, W.R., Kozuch, M., Brito Neves, B.B., 2011. Precambrian history of the Zona Transversal of the Borborema Province, NE Brazil: insights from Sm-Nd and U-Pb geochronology. J. S. Am. Earth Sci. 31, 227–252.
Van Schmus, W.R., Oliveira, E.P., Da Silva Filho, A., Toteu, S.F., Penaye, J., Guimarães, I.P., 2008. Proterozoic Links between the Borborema Province, NE Brazil, and the Central African Fold Belt, vol. 294. Geological Society, London, Special Publications, pp. 69–99.
Whitmarsh, R.B., Manatschal, G., 2012. Evolution of magma-poor continental margins from rifting to seafloor spreading. In: Roberts, B.G., Bally, A.W. (Eds.), Regional Geology and Tectonics: Phanerozoic Passive Margins, Cratonic Basins and Global Tectonic Maps, vol. 1C. Elsevier, Amsterdan, pp. 326–341.
Whitmarsh, R.B., Manatschal, G., Minshull, T.A., 2001. Evolution of magma-poor continental margins from rifting to seafloor spreading. Nature 413, 150–154.
Wood, D.A., 1980. The application of a Th-Hf-Ta diagram to problems of tectonomagmatic classification and to establishing the nature of crustal contamination of basaltic lavas of the British Tertiary volcanic province. Earth Planet. Sci. Lett. 50, 11–30.